JOURNAL OF GEOPHYSICAL RESEARCH, VOL. 111, E09002, doi:10.1029/2006JE002703, 2006

Click Here for Full Article

Io: Loki Patera as a magma sea

Dennis L. Matson,[1] Ashley Gerard Davies,[1] Glenn J. Veeder,[1] Julie A. Rathbun,[2] Torrence V. Johnson,[1] and Julie C. Castillo[1]

Received 15 February 2006; revised 31 March 2006; accepted 17 May 2006; published 2 September 2006.

[1] We develop a physical model for Loki Patera as a magma sea. We calculate the total volume of magma moving through the Loki Patera volcanic system every resurfacing cycle (~540 days) and the resulting variation in thermal emission. The rate of magma solidification at times reaches 3×10^6 kg s^{-1}, with a total solidified volume averaging 100 km^3 yr^{-1}. A simulation of gas physical chemistry evolution yields the crust porosity profile and the timescale when it will become dense enough to founder in a manner consistent with observations. The Loki Patera surface temperature distribution shows that different areas are at different life cycle stages. On a regional scale, however, there can be coordinated activity, indicated by the wave of thermal change which progresses from Loki Patera's SW quadrant toward the NE at a rate of ~1 km d^{-1}. Using the observed surface temperature distribution, we test several mechanisms for resurfacing Loki Patera, finding that resurfacing with lava flows is not realistic. Only the crustal foundering process is consistent with observations. These tests also discovered that sinking crust has a "heat deficit" which promotes the solidification of additional magma onto the sinking plate ("bulking up"). In the limiting case, the mass of sinking material can increase to a mass of ~3 times that of the foundering plate. With all this solid matter sinking, there is a compensating upward motion in the liquid magma. This can be in excess of 2 m yr^{-1}. In this manner, solid-liquid convection is occurring in the sea.

Citation: Matson, D. L., A. G. Davies, G. J. Veeder, J. A. Rathbun, T. V. Johnson, and J. C. Castillo (2006), Io: Loki Patera as a magma sea, *J. Geophys. Res.*, *111*, E09002, doi:10.1029/2006JE002703.

1. Introduction

[2] Loki Patera is perhaps the most distinctive feature on Io. It has changed little since it was discovered by Voyager (Figure 1) [*Smith et al.*, 1979a; *McEwen et al.*, 1998]. It is a generally circular feature, approximately 200 km in diameter, centered at 309.9°W longitude, 12.6°N latitude. It constitutes about 0.07% of Io's surface area. The dark material at Loki Patera contrasts strongly with the higher albedo surroundings. The Loki Patera volcanic area accounts for 10 to 20 percent of the total heat flow from Io [*Veeder et al.*, 1994]. It is Io's largest source of volcanic thermal emission. Although the initial Voyager and Infrared Telescope Facility (IRTF) observations had insufficient spatial resolution to conclusively associate the dark material with the Loki hot spot's thermal emission, subsequent studies of the relationship of albedo and volcanic heat sources [*McEwen et al.*, 1985] and spatially resolved Galileo data from the Near Infrared Mapping Spectrometer (NIMS) and Photopolarimeter-Radiometer (PPR) demonstrated that the visually dark regions are indeed the source of thermal emission [*McEwen et al.*, 1985; *Geissler et al.*, 1999; *Lopes-Gautier et al.*, 2000; *Spencer et al.*, 2000; *Davies*, 2003; *Lopes et al.*, 2004]. About 200 km to the north of Loki Patera is the source of the large, intermittent Loki plumes that were active during the Voyager epoch, indicating substantial surface or near-surface volatile deposits in that location.

1.1. Why Study Loki Patera?

[3] We have two motivations for investigating Loki Patera. It is the biggest structure of its type on Io, and it has been classified as the end-member for this type of volcanism [*Veeder et al.*, 1994]. Here we expect that the underlying processes of these volcanoes will be most clearly expressed. Loki Patera's large areal extent allows us to study its surface and geologic processes many tens of kilometers from its edges where other effects may also be present. When we have achieved an understanding of the main processes away from the margins of Loki Patera, we will be better equipped to study the more complicated situations that arise at the margins.

[4] Our second motivation is to find out how Io's observed heat flow is generated and released. Thus it makes sense to go where heat flow from the surface is high, and Loki Patera is the largest single source of heat flow on Io [*Veeder et al.*, 1994]. We conjecture that the very large amount of heat coming out of Loki Patera means that Loki Patera must be well-connected to the source. However, the

[1] Jet Propulsion Laboratory, Pasadena, California, USA.
[2] Department of Physics, University of Redlands, Redlands, California, USA.

Copyright 2006 by the American Geophysical Union.
0148-0227/06/2006JE002703$09.00

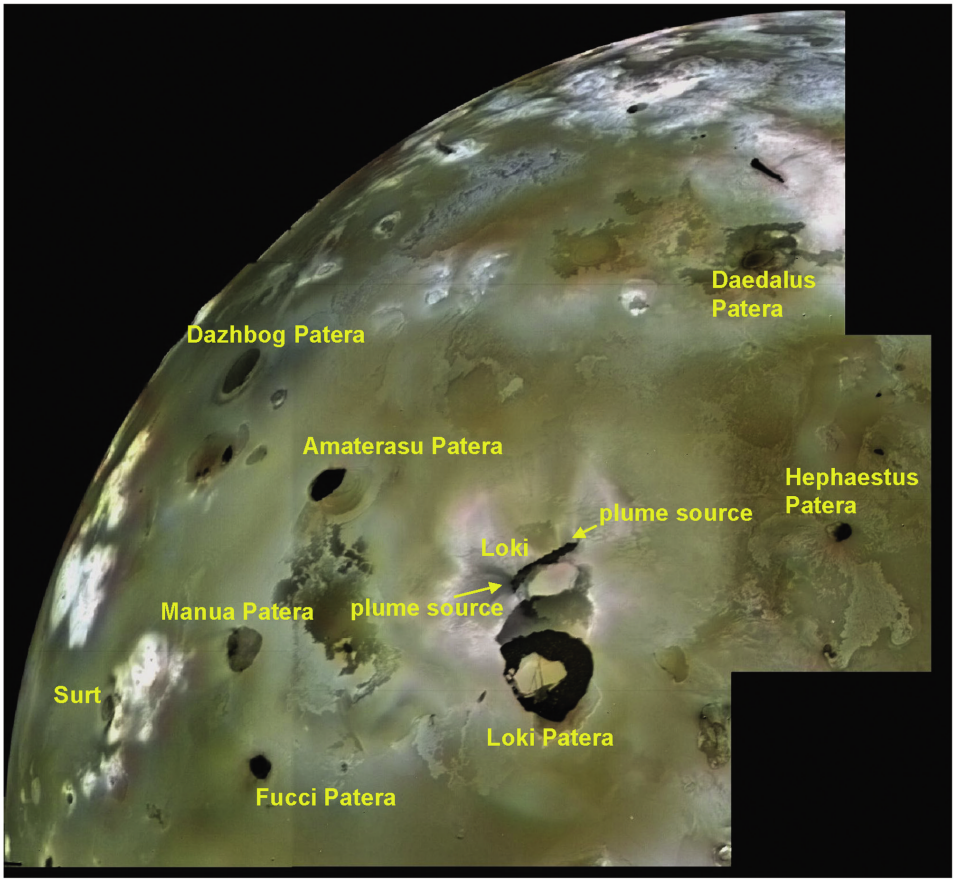

Figure 1. Loki Patera as seen by Voyager 1 in March 1979. Numerous volcanic calderas and lava flows are visible. Loki Patera is the large shield-shaped black feature in the lower center and is about 200 km in diameter. The bright whitish patches are probably freshly deposited SO_2 frost. The feature Loki was the source of two volcanic plumes during the Voyager epoch. Photo credit: NASA.

requirement for transporting so much heat through a conduit is staggering.

1.2. Why a New Model?

[5] Previous authors have more or less exhausted the possibilities of styles of volcanic activity at Loki Patera using morphological and volcanological comparison with terrestrial analogues, and relatively simple models [*Lunine and Stevenson*, 1985; *Carr*, 1986; *Davies*, 1996, 2001, 2003; *Howell*, 1997; *Lopes-Gautier et al.*, 2000; *Spencer et al.*, 2000; *Rathbun et al.*, 2002; *Gregg and Lopes*, 2004]. In order to advance further we need to use a quantitative, physical model, which will facilitate numerical simulations of processes operating in Loki Patera [e.g., *Carr*, 1986]. With it we can use the power of physics, chemistry, and geology, to study Loki Patera in three spatial dimensions and time. In this paper, as we investigate the surface of Loki Patera, we will show that our model and its simulations give us a better understanding of the observational data, and better knowledge of the operative processes, allowing us to formulate quantitative predictions.

1.3. What's Ahead in This Paper?

[6] We start our discussion of the expression of volcanic activity at Loki Patera by tackling the type of volcanism that occurs there. Sulfur, basaltic and ultramafic magmas have been advanced as candidates. We show that basalt is the best candidate magma for Loki Patera. We evaluate the strengths and weaknesses of two of the primary possible resurfacing mechanisms, lava flows versus a lava lake. Our proposed "Magma Sea" model is then defined. The formation of crust that floats on its surface is treated in detail. A portion of sea crust is quantitatively followed through its entire life cycle, from its creation as magma exposed at the surface of the sea to its demise by foundering. We model the thermal emission from our crust formation model and compare this with observations. Finally, we consider the effects on the crust of dissolved gas and degree of crust porosity, and the process of "bulking up," or accretion of more crust through magma solidification, is described.

[7] In addition to the dark areas of Loki Patera (as seen in Figure 1) there are also brighter albedo areas, variously described as "islands," "icebergs," and thin surface deposits, which do not exhibit significant thermal emission [*Lopes-Gautier et al.*, 2000]. The formation and evolution of these less-active surfaces and their influence on the magma sea are not included in this paper.

[8] There are two appendices. Appendix A describes the relationship between lava surface age and temperature. Appendix B describes how this information is used to

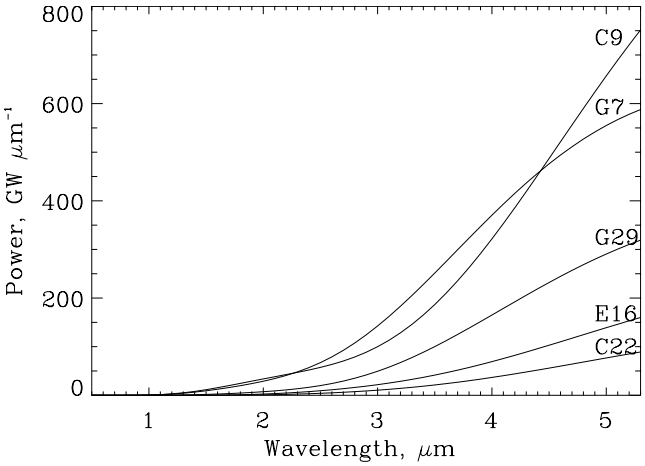

Figure 2. NIMS observations of Loki Patera in darkness at low spatial resolution. Note the low thermal emission at short wavelengths (<1.5 μm) and the curves rising toward their peaks in the mid-infrared. Observation identifiers are given in Table 1. After *Davies* [2003].

model the evolving thermal emission from an overturning lava lake.

2. Silicate Volcanism at Loki Patera

[9] The literature immediately following the Voyager flybys of the Jupiter system focused on sulfur driven volcanism at Io [e.g., *Smith et al.*, 1979a, 1979b; *Sagan*, 1979]. This was a consequence of Io's vivid colors which were thought to be due to various allotropic forms of sulfur [e.g., *Sagan*, 1979]. Some authors suggested both sulfur and silicate volcanism were present [e.g., *Carr*, 1986] and the evidence continued to accumulate that pointed to silicate magma dominating Io's volcanism. However, sulfur may play a secondary role near the surface [e.g., *Greeley et al.*, 1984; *Williams et al.*, 2001].

[10] Observed temperatures at Loki Patera are indicative of silicate volcanism. Temperatures derived from two-temperature fits to low-spatial resolution NIMS data (Figure 2) are at least ~990 K (Table 1), too high for predominantly sulfur volcanism at Loki Patera [*Davies*, 2003], but consistent with inferred silicate-range temperatures from ground-based data [*Johnson et al.*, 1988] at, or in the vicinity of, Loki Patera. The uncertainty in location is important because thermal emission from a nearby silicate eruption could add short-wavelength thermal emission to that of low-temperature sulphur-dominated volcanism in Loki Patera. The matter was resolved when both NIMS and the Galileo Solid State Imaging experiment (SSI) observed Loki Patera almost simultaneously on 28 June 1997. The NIMS spatial resolution was low, at 725 km per pixel. It was feasible that the large area covered by each NIMS pixel might include emitting centers other than Loki Patera, such as from Amaterasu Patera. However, SSI detected thermal emission from Loki Patera in an eclipse observation, implying temperatures in excess of 700 K, and no other hot spot in the area covered by NIMS in the vicinity of Loki Patera was emitting at this temperature at that time [see *McEwen et al.*, 1998; *Lopes-Gautier et al.*, 1999]. The hot component (960 K) seen by NIMS during June 1997 was therefore located at Loki Patera and indicated that the primary volcanism occurring at Loki Patera is silicate.

[11] Additionally, the Cassini Imaging Sub-System (ISS) detected thermal emission from Loki Patera, indicating surface temperatures of at least 700 K [*Davies et al.*, 2001]. The infrared fluxes observed remotely do not easily yield the melt temperature of the liquid magma itself directly, but rather result from a mixture of emissions from cooling lava at various temperatures, and probably very small areas of fresh magma, briefly exposed [*Flynn and Mouginis-Mark*, 1994; *Davies*, 1996; *Keszthelyi and McEwen*, 1997]. Derived temperatures from a two-temperature fit are not necessarily magma liquidus temperatures but instead may underestimate liquidus temperature by several hundred K or more [*Flynn and Mouginis-Mark*, 1994].

[12] If Loki Patera is, as we believe, a molten magma sea, still higher temperatures will be found below the surface crust. These higher temperatures are seen from time to time when the crust founders, and through cracks in the crust.

3. Eruption Style and Surface Renewal at Loki Patera

3.1. Resurfacing With Lava Flows

[13] The surface of Loki Patera is periodically renewed and we start our study by identifying the most likely process by which the surface of the patera floor is replaced. Previously, workers, cited in Section 2 above, have proposed different mechanisms described below for resurfacing Loki Patera, but the similarity in integrated thermal emission spectra from these processes prevented unambiguous identification of the responsible mechanism. Possible resurfacing mechanisms for Loki Patera include Model 1 (Figure 3a) covering the patera floor with new lava flows; Model 2 (Figure 3b), the "mobile crust" model where new

Table 1. Two-Temperature Fits to Galileo Low-Resolution NIMS Loki Patera Data[a]

Galileo Orbit	Observation	Date	Temperature of "Hot" Area, T_H, K	"Hot" Area A_H, km^2	Temperature of "warm" Area, T_W, K	"Warm" Area A_W, km^2	Total Thermal Output, 10^{12} W
G7	G7INVOLCAN05	05APR97	990	3	460	2320	6.1
C9	C9INCHEMIS06	25JUL97	962	5	373	11700	13.0
E16	16INHRSPEC01	21JUL98	612	27	345	3830	3.3
C22	22INHRSPRC01	14AUG99	576	21	339	2420	1.9
G29	29INIWATCH03	28DEC99	878	2	417	2330	4.1
						Average	**5.7**

[a]After *Davies* [2003].

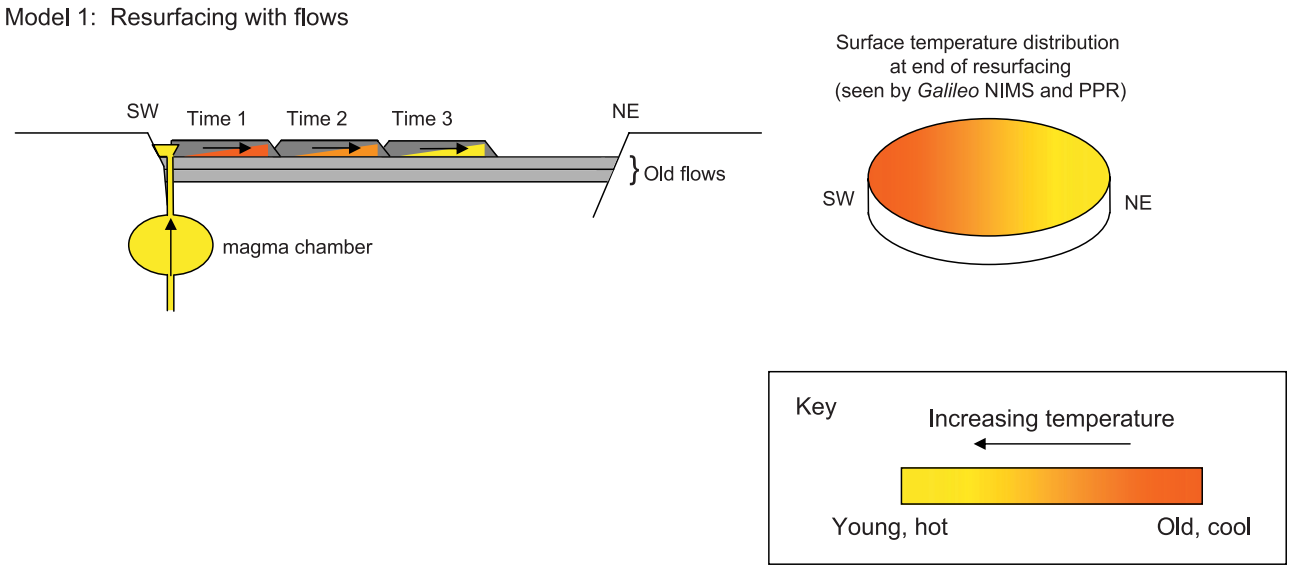

Figure 3a. Figures 3a, 3b, and 3c show three different types of resurfacing discussed in the text. The resulting temperature distribution for each model is compared to NIMS and PPR observations. Model 1 illustrates resurfacing with lava flows.

hot magma is exposed behind a moving plate of older, cooler material; and Model 3 (Figure 3c), the "foundering model," where lava lake surface is renewed by sinking of the crust and its replacement with newly solidified lava. Each of these processes has a surface temperature distribution signature, as illustrated in Figures 3a–3c, which changes with time. These signatures are compared to each other and to observed temperature distributions from Galileo NIMS data [*Davies*, 2003]. Lava flows (i.e., Model 1, Figure 3a) and sinking rafts (Model 3, Figure 3c) have signatures consistent with Galileo NIMS data [*Davies*, 2003], while (Model 2, Figure 3b) does not. These resurfacing mechanisms are now considered in more detail.

[14] The NIMS data show a more-or-less smoothly increasing temperature trend from the southwest corner of Loki Patera toward the northeast [*Davies*, 2003], similar to that seen earlier in PPR observations [*Spencer et al.*, 2000]. If resurfacing was by emplacement of flows, then they would have to (1) spread across the entirety of the patera floor without forming channels, (2) advance with a constant rate of areal coverage, and (3) cease precisely, when the entire floor has been resurfaced. This cycle would then have to repeat periodically. To produce the observed temperature distribution, flows would originate in the SW corner of Loki Patera, form lobes with cooling crusts, which would inflate. Breakouts of fluid lava would form new flow lobes and the process would repeat, advancing cross the floor of the Patera. The previously formed crust would be left in place. This process is observed on Earth on a much smaller areal scale during eruption of low-viscosity basalt flows. Harder to explain is the required constant areal coverage rate, implying a constant volumetric eruption rate, and the covering of the entire floor of the Patera, which is not conducive to directional flows because it appears to have a flat, non-inclined surface [*Geissler et al.*, 2004]. Furthermore, no individual flow units have been seen at Loki Patera. To the resolution of available data, Loki Patera appears to be flat, so flat that it exhibits specular reflectance at appropriate viewing geometries (Figure 4) [*Geissler et al.*, 2004; *Turtle et al.*, 2004]. Thus, if resurfacing is done by flows it requires that the lava flow process occur in a way that is distinctly uncharacteristic of lava flows.

3.2. Resurfacing of a Lava Lake

[15] The destruction of the crust on a lava lake on Earth may be through either subduction or foundering of a mobile crust. We designate these modes of crust renewal as the "mobile" and "foundering" models. Foundering occurs when the crust bulk density exceeds that of the liquid lava [*Rathbun et al.*, 2002] and will be discussed later. Subduction, as in the "mobile" model, is analogous to plate tectonics, where crustal plates appear to slide across the surface of molten magma and descend upon reaching the caldera wall. A well-documented terrestrial example is the lava lake at Kupaianaha, Hawai'i that was active continuously from July 1986 until August 1990. For much of this time the lava lake experienced constant, semi-periodic overturning followed by the formation of a thick, stable, immobile, crust. The crustal "plates" were destroyed at an active margin where they were subducted beneath the surface [see *Flynn et al.*, 1993]. In a lava lake, the movement and destruction of surface crust is driven from below by convection of magma within the lake. We discuss details of the mobile and foundering crust models below.

3.2.1. "Mobile" Crust Model, Variation 1

[16] Assuming that the crust is destroyed in the southwest corner of the patera, the plates would be carried toward the SW where they break up at the SW margin. On the other side of the patera, new material would be exposed as the plates draw away from the caldera wall. The newly forming crust is attached to the caldera wall and does not move as a unit. The resulting temperature trend across the Patera has younger and hotter surfaces toward the SW, the reverse of what NIMS saw [*Davies*, 2003]. The implied movement

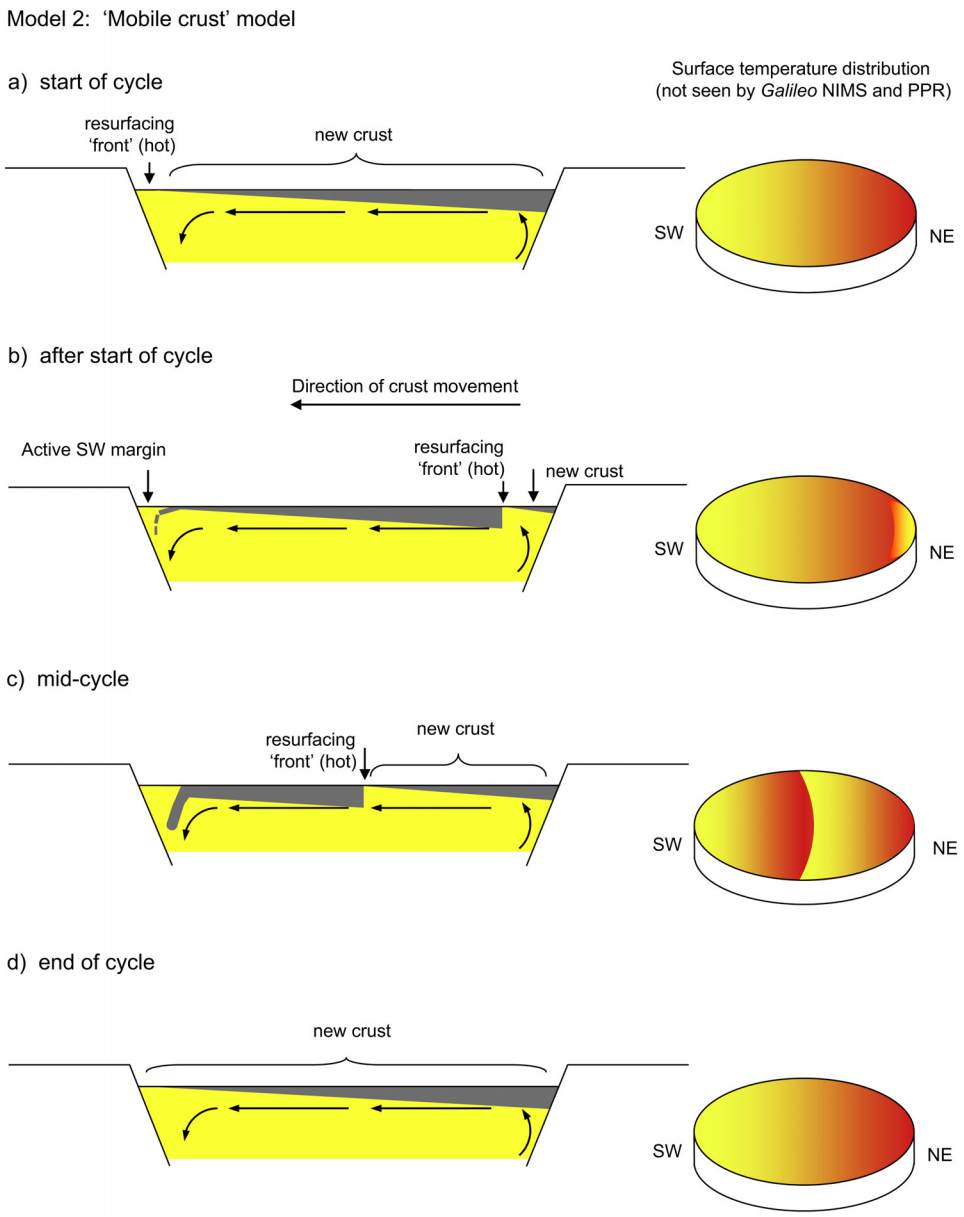

Figure 3b. Model 2 shows the replacement of lava lake crust using a "mobile" crust model akin to plate tectonics.

toward the NE of a hot margin is the reverse of what is seen in PPR data (Figure 3b).

3.2.2. "Mobile" Crust Model, Variation 2

[17] Conversely, the subduction could occur in the NE, pulling the crust away from the SW corner toward the NE. At the other end of the Patera, starting in the SW, new material would first be exposed as the plate draws away from the caldera wall. This mechanism would theoretically reproduce the temperature distribution observed by NIMS, but relies on a hot, emitting source in the NE where crust is being destroyed. At the height of the 1997 brightening, SSI only saw a thermal source in the southern half of Loki Patera [*McEwen et al.*, 1997].

[18] Since at the start the mobile models require all of the surface elements to move in concert, it is difficult to see how the nearly linear recycling front would be maintained and propagated over distances approaching 200 km. This would seem to require that Loki Patera have a complex, highly coordinated system of convection cells below its surface. Galileo PPR data indicated that the resurfacing of Loki Patera between October 1999 and February 2000 was taking place at a rate of $\sim$1 km d^{-1} [*Spencer et al.*, 2000]. The velocity of the "subduction" wave suggests that in the mobile plate model the recycling time for Loki Patera should be $\sim$200 days, rather than the observed $\sim$500 to 600 days.

3.2.3. Foundering Model

[19] In the foundering crust model [*Davies*, 2001; *Rathbun et al.*, 2002], the crust forms in place, thickens with time, and eventually sinks in situ when its bulk density surpasses the density of the liquid sea.

[20] This resurfacing process relies solely on the radiation of heat by thermal emission and the consequential formation of a crust on the sea. It is therefore free from all of the

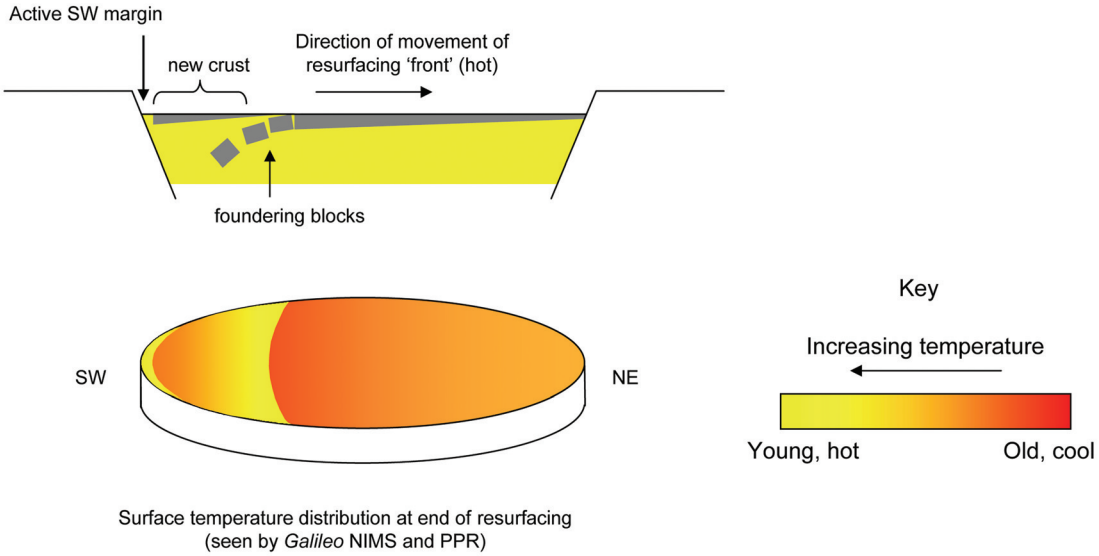

Figure 3c. Model 3 is the "foundering" model [after *Rathbun et al.*, 2002].

complex interplay of processes that accompany the supply to, and eruption of, magma from subsurface reservoirs. It is also free of all of the complexities needed for mobile crust transport and interactions with the boundaries of Loki Patera. The surface of the sea continually renews itself. Foundering, when crust bulk density exceeds the density of the magma beneath, is inevitable, and yet the simplicity of the process allows detailed constraints to be placed on the physical parameters and on the mechanism by which magma reaches the surface.

[21] *Davies* [2003] demonstrated that the temperature distribution on the floor of Loki Patera in October 2001 was consistent with this model, with the oldest crust adjacent to the active area in the SW corner of Loki Patera, with the surface, in general, getting progressively younger toward the NE, indicative of a resurfacing front moving diagonally across the patera at a rate of roughly 1 km per day (Figure 5) in a manner very much like that seen by PPR [*Spencer et al.*, 2000]. The resurfacing front implies coordinated or coupled activity between surface plates and this can be accommodated by the model.

4. Defining the "Magma Sea" Model

[22] We present a model that provides the overall framework for our investigation of Loki Patera. From this model various simulation studies are launched to explore specific volcanic processes. The simulations provide the basis for comparing our model results with observation and for developing predictions for what has not or cannot be measured with the present technology.

[23] We model Loki Patera as a large, outwardly quiescent body of basaltic magma approximately 200 km in diameter and a presently unknown depth. To illustrate the size of this "sea" of magma on a global scale, we note that the surface has significant curvature and follows the hydrostatic shape for Io. The local horizon is set by this curvature. An observer looking from a height of 1.5 m above the surface sees the horizon at a distance of 2.3 km away. Taking advantage of this large scale, we model processes affecting the magma in the middle of the dark area of the patera "floor," the crust and the near-surface magma

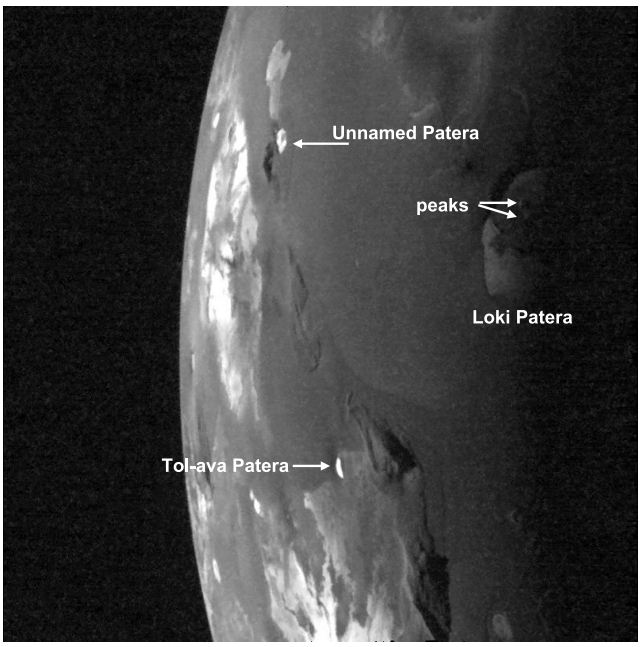

Figure 4. Loki Patera as seen in a low-sun angle image obtained by Galileo SSI on 16 October 2001. The image has a resolution of 1.1 km pixel^{-1}. North is to the top of the picture. The material on the floor of Loki Patera exhibits specular reflectivity [*Geissler et al.*, 2004; *Turtle et al.*, 2004], implying a smooth, possibly glassy surface. The same effect is observed with the crusts that form on quiescent basalt lava lakes on Earth [see *Wright and Okamura*, 1977]. On the Loki Patera "island," two small peaks are seen. NASA image PIA03530.

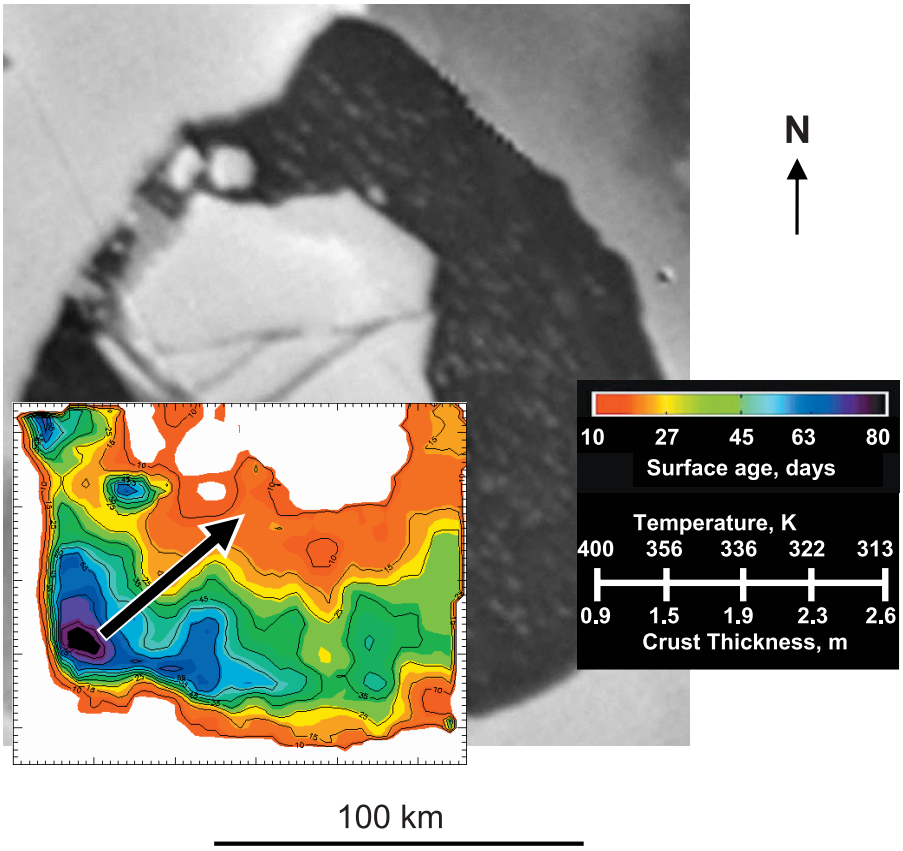

Figure 5. Image of Loki Patera showing the *Davies* [2003] temperature map with the location and inferred direction of motion of the resurfacing front noted. Also shown is the age of the surface and the crustal thickness. The active front, where crust is foundering and being replaced by new, hot lava, is probably to the NE of the area covered by the Galileo NIMS observation 32INTHLOKI01 obtained in October 2001 from which the *Davies* [2003] age-temperature map was derived.

beneath. We assume that the shore does not interact with the sea other than to define its boundary. Similarly, we assume that the sea is "deep" and the boundary at its bottom is inert. The tenuous atmosphere of Io has no effect on the magma sea. The model's upper surface is the observable magma whether it be liquid or solidified as sea crust. In general, the sea surface is very smooth, a fact supported by a Galileo image showing a specular reflection from the surface (Figure 4). This means that the sea is isostatic and has very little if any topography.

[24] The initial condition is isothermal and static. The magma is assumed to be 1475 K, liquidus temperature for a typical Hawaiian basalt [*Wright et al.*, 1968].

[25] The (approximately) isothermal state can be maintained indefinitely. Although initially static, the simulations show us that mass motion starts immediately. Mass transport is involved initially in making the sea crust and later in its foundering and in the convection that is thereby initiated. Elements of the sea are also moved vertically and horizontally by the diurnal tides. The sea has no ad hoc subsurface structures or "plumbing" such as magma conduits and reservoirs or chambers, which are characteristic of terrestrial, lava-lake analogues.

[26] The term "magma sea" was chosen for two reasons. First, it is appropriate because Loki Patera is larger than a typical "lake" and smaller than a typical "ocean." Second, the term is relatively fresh, compared to "magma ocean," and "lava lake" which have been used extensively in the literature, and bring forth images that are different than the one we wish to convey for Loki Patera.

[27] These model assumptions are sufficient for our present purpose. Obviously, all of the assumptions could be treated more precisely and/or accurately. Later, after we know more about the sea there may evolve reasons that justify the effort needed to treat some of the assumptions more rigorously and with a more advanced modeling.

5. Forming the Crust

[28] For our study of resurfacing we have chosen a location in the center of the Loki Patera sea (the middle of the low-albedo area). Resurfacing is cyclic [e.g., *Rathbun et al.*, 2002] and we will start our description at the point in the cycle where some plates of sea crust have foundered and have just been replaced at the surface by liquid magma. The newly exposed lava forms a relatively smooth, level surface. It radiates heat very intensely. The surface cools rapidly, forming, almost instantly, a very thin, glassy, skin, that may be responsible for the observed specular reflection from Loki Patera (see Figure 4). We next discuss formation of this crust in terms of specific details of its thickness and gas content, and the effect on porosity and density.

Table 2. Basalt Physical and Model Parameters

Property	Symbol	Value	Units
Latent heat of crystallization	C_L	4×10^5	J kg^{-1}
Specific heat	c_p	1500	J kg^{-1} K^{-1}
Liquidus temperature	T	1475	K
Lava solid density	ρ_{sol}	2800	kg m^{-3}
Lava liquid density	ρ_{liq}	2600	kg m^{-3}
Thermal conductivity	k	0.9	W m^{-1} K^{-1}
Emissivity	ε	0.9	W m^{-2} K^{-4}

5.1. Crustal Thickness

[29] The heat being lost to space comes from the cooling and solidifying lava. Temperatures for the surface of the crust and its interior have been calculated using established methods [*Davies*, 1996; *Davies et al.*, 2005] using thermophysical parameters for basalt given in Table 2. The relationship between surface age and temperature, critical to determining thermal emission as a function of time for each resurfacing model, is described in Appendix A. The cooling of basalt on Io's surface is shown in Figure 6. The total heat radiated from the surface comes from the release of latent heat from magma solidifying on the bottom of the sea crust (and to a lesser extent from the cooling of crust that has already formed and from the absorption of sunlight).

[30] Thus, to a good approximation, the rate at which the thickness of the sea crust grows is directly proportional to the power radiated by thermal emission. Approximately 30 hours after emplacement, the sea crust reaches a temperature of 500 K and has grown about 32 cm [*Davies et al.*, 2005]. Further, the rate of growth on the bottom of this slab (Figure 7) is about 1 micron per second. By contrast, the oldest crust at Loki Patera (based on a 540-day residency [*Rathbun et al.*, 2002]) has a surface temperature of ~250 K and a thickness of ~7 m. The rate of growth has now dropped to 4×10^{-8} m s^{-1} (equivalent to ~1.3 m yr^{-1}). Crustal growth rate as a function of time is also shown in Figure 7.

5.2. Gas Content

[31] The concentration of dissolved gas at depth determines how much gas will eventually exsolve as the magma comes to the surface. Pressure is also a major factor determining the size of the bubbles or vesicles formed and thus the porosity of the layers newly forming on the bottom of the crust. For a thin crust the pressure at the bottom will be relatively low and a relatively porous crust layer forms. If the crust is thick, the bubbles below it will not be as abundant and the layer will have a density closer to that of solid rock. Solid rock is ~10% more dense than its melt, and as more and more solid lava accretes onto pre-existing crust, crust bulk density increases and eventually the crust becomes negatively buoyant and sinks [*Rathbun et al.*, 2002].

[32] Recurrent brightening of Loki Patera in the 3–20 μm wavelength range has been analyzed using heat transfer models [*Davies*, 1996; *Howell*, 1997]. These yield ~7 m as a typical estimate for the thickness of the crust after ~500 days. For the purpose of modeling crustal formation we bracket this by calculating models for terminal thicknesses of five and ten meters. These thicknesses compare well with a terrestrial analogue. From measurements of porosity of the crusts of the Alae and Makaopuhi lakes, Hawaii [*Wright and Okamura*, 1977]. *Rathbun et al.* [2002] estimated that crusts would become gravitationally unstable when thicknesses of ~6 m were reached.

[33] The formation of porous crust can also be considered from a physical chemistry point of view. The SO_2 content of the magma in the sea must be relatively low. If it were high, explosive degassing would continually disrupt the crust on the magma sea and lead to randomly spaced, high-temperature hot spots. These hot spots are not observed at Loki Patera [*Davies*, 2003]. The solubility of SO_2 in basaltic magma has been considered by *Leone and Wilson* [2001]. Using their formulation for solubility as a function of pressure, we have calculated the resulting profile for a given

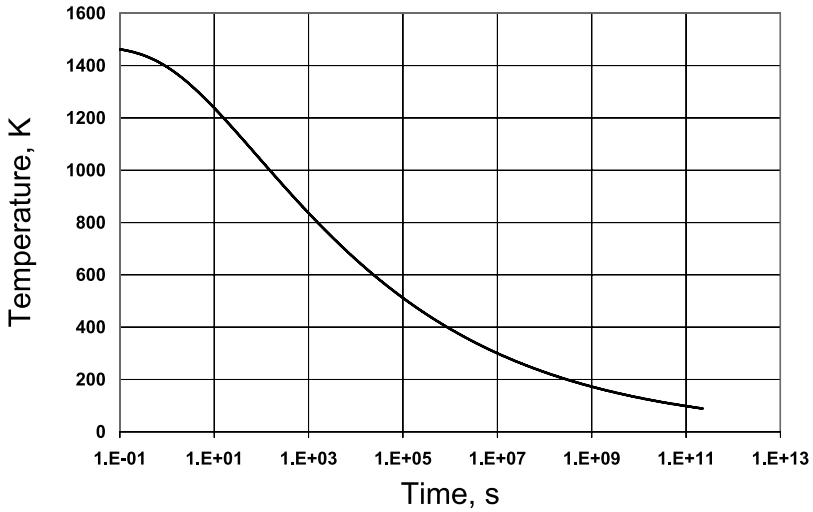

Figure 6. Cooling of the surface of a basalt lava body on Io [*Davies et al.*, 2005]. The black curve is for a semi-infinite body. An areally extensive, deep lava lake is such a body. Heat loss from the lava, conducted through a surface crust that thickens with time, is buffered by the liberation of latent heat from solidifying lava. The basalt thermophysical properties used in this paper are shown in Table 2.

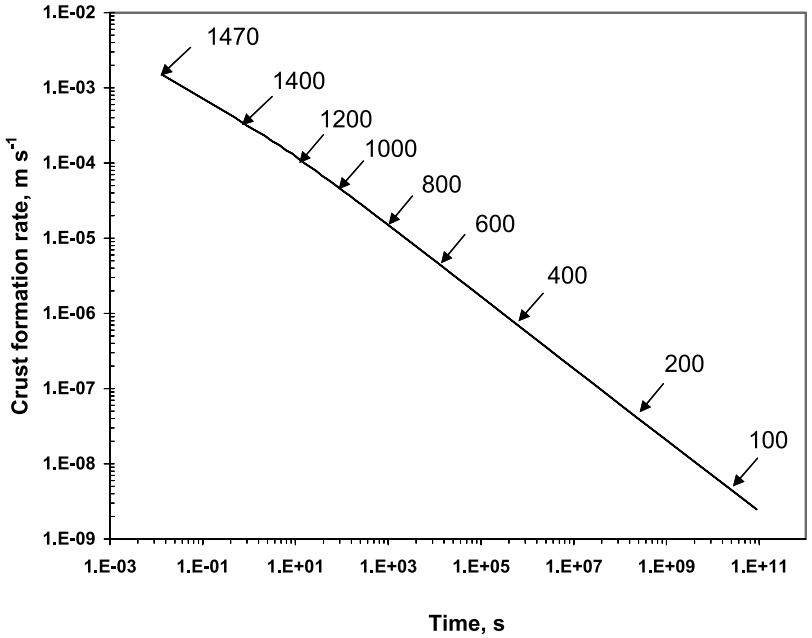

Figure 7. Crust growth versus time for a semi-infinite magma body on Io as a function of surface temperature [*Davies et al.*, 2005]. Basalt thermophysical properties used are shown in Table 2. Crust formation rate decreases rapidly with surface temperature. Arrows point to the time since exposure for different values of surface temperature, given in K.

amount of dissolved SO_2. Profiles of porosity with depth for crust thicknesses of 5 and 10 m are shown in Figure 8.

[34] With an abundance of SO_2 on Io and, so far, non-detections of other typical terrestrial volcanic gases such as H_2O and CO_2, it is reasonable to assume that SO_2 is the gas chiefly responsible for the porosity of Ionian lavas. *Leone and Wilson* [2001] considered the matter of porosity for volcanic deposits on Io. They noted that a reasonable range for porosity would be 30–40%, and adopted 30% for their calculations. They also collected current knowledge about the solubility of SO_2 in basalt and found it to be sparse. Using *Mysen*'s [1977] data for an albite melt they developed the following expression to use for the equivalent saturation mass fraction, n, of SO_2 in basalt:

$$n_{SO2} = 7.5 \times 10^{-12}\, P - 2.6 \times 10^{-21}\, P^2 + 3.2 \times 10^{-31}\, P^3, \quad (1)$$

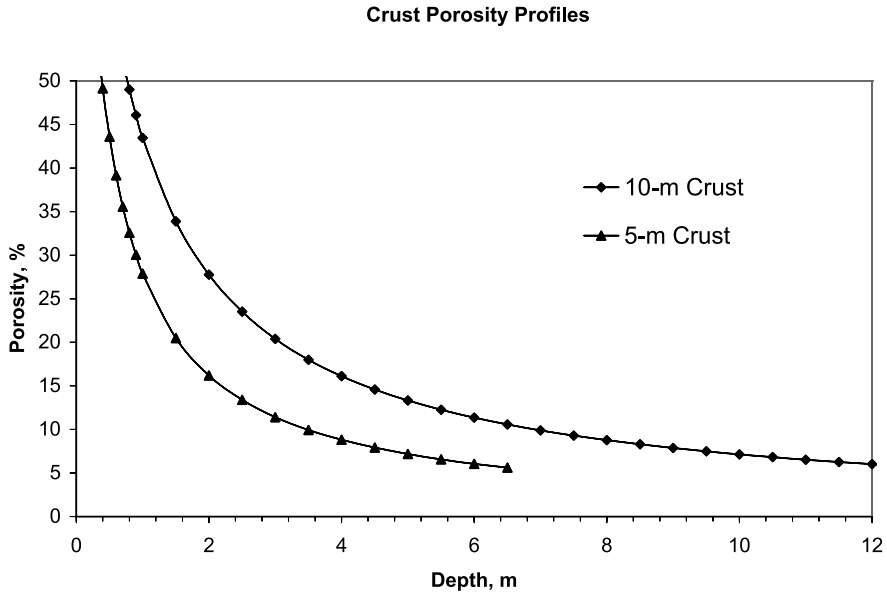

Figure 8. Theoretical vertical porosity profiles for sea crust which become neutrally buoyant at thicknesses of 5 and 10 m. Properties are as in Table 3. Porosities above 50% are not shown because near-surface conduction prevents the higher porosities from being achieved.

Table 3. Crust Properties

Parameter	5 m Thick Crust	10 m Thick Crust
n_{SO2}	1.82×10^{-5}	3.62×10^{-5}
40% porosity depth	0.5 m	1 m
30% porosity depth	0.9 m	1.5 m

where P is pressure in Pa. At high pressure (e.g., above 300 MPa, a depth of ~60 km) the magma saturates at a SO_2 fractional mass of between 0.5 and 1%. At the pressures of interest in our study, the fractional mass of dissolved SO_2 declines very rapidly with pressure. From equation (1), and also by inspection of Figure 8, it can be seen that as magma rises, SO_2 will be largely exsolved by the time depths of interest are reached. This relationship between crust porosity, SO_2 content and pressure can be illustrated as follows. At a depth of 1 km the pressure is 4.7 MPa and $n_{SO2} = 3.5 \times 10^{-5}$. Between this depth and the surface the total content of remaining SO_2 is about ten percent of this number. Thus, as we build the thickness of the crust, the additional amount of exsolving gas is relatively minor and we ignore it.

[35] After the initial emplacement of liquid lava and the flash freezing of its surface, the sea crust continues to grow below the surface. Latent heat of solidification is conducted upward through the crust and radiated to space. The porosity, φ, of the solidifying layer can be calculated from:

$$\varphi = v_{SO2}/(v_{melt} + v_{SO2}), \tag{2}$$

where v_{melt} represents the specific volume of a kilogram of basalt magma (at zero porosity) which is 3.57×10^{-4} m^3 and v_{SO2} is the specific volume in the magma, given by

$$v_{SO2} = v_{STP\text{-}SO2}\, p_{STP}/P, \tag{3}$$

where $v_{STP\text{-}SO2}$ is the specific volume of SO_2 at standard temperature and pressure (i.e., $[n_{SO2}/64$ kg-mole$^{-1}] \times 22.4146$ m^3 kg-mole^{-1}), p_{STP} is 1.01325×10^5 Pa, and P is the pressure for which the porosity φ is being calculated.

[36] Given a value for n_{SO2}, it is possible to calculate a porosity profile for the crust. It turns out that the crustal thickness itself is sufficient to constrain the mass fraction of gas in the magma. We solved for n_{SO2} iteratively by means of calculating the buoyancy. We found the value of n_{SO2}, which gave neutrally buoyant sea crusts for thicknesses of 5 and 10 m. This was done by comparing the mass of a column of sea crust with an equivalent column of liquid basalt. Strictly speaking, the reference column should also allow for the presence of vesicles in the magma. However, this was ignored since this effect only starts to be significant at depths of less than a meter (see Table 3; Figure 8).

[37] We adopt the 30–40 percent porosity noted by *Leone and Wilson* [2001] as a practical guideline. The high porosities at shallow depths indicated by the theoretical expressions derived by *Leone and Wilson* [2001], are not achieved. This is due, mainly, to these expressions not including the viscoelastic properties of the magma.

[38] *Leone and Wilson* [2001] noted that exsolution of SO_2 starts at 70 MPa or a depth of about 16 km. *Sparks* [1978] reviewed the micro-conditions under which bubble nucleation could take place. Nucleation occurs readily in basalt. The key parameter is the radius for a "critical nucleus." If the bubble is smaller than this critical size it will shrink spontaneously while those that are larger will grow spontaneously. By inspection of curves presented by *Sparks* [1978, Figure 1] we chose 10 microns as the critical radius.

[39] For an ideal gas, the bubble radius scales as

$$R = R_o\,(P_o/P)^{1/3}. \tag{4}$$

Letting bubbles exsolve at 16 km depth (7.49×10^7 Pa) with a critical radius of 10 microns, the above equation is used to plot bubble radius as a function of depth (Figure 9). The bubbles remain relatively small, reaching a radius of only about a millimeter at a depth of a centimeter in the magma sea. In most cases they will be trapped by solidification at the bottom of the crust and not be able to reach depths as shallow as a centimeter. However, when

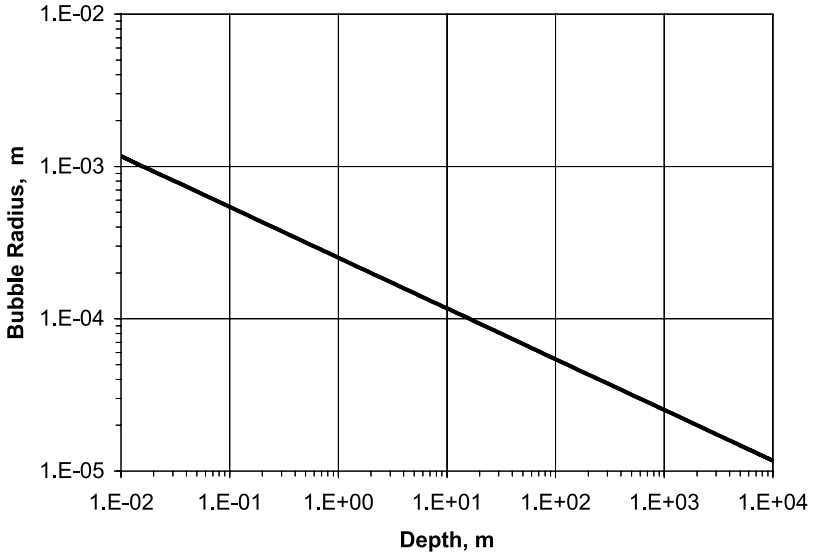

Figure 9. Bubble radius versus depth for exolved SO_2.

part of the crust sinks, molten magma is exposed at the surface where pressure is effectively nil. What stops the bubbles' expansion?

[40] As the bubbles expand isothermally they absorb heat and cause a small amount of magma to solidify. This can be calculated from the work done w (in Joules) such that

$$w = RT\ \ln(p_1/p_2), \tag{5}$$

where p_1 is the pressure at 16 km depth and p_2 is the pressure at 1 cm. The work done causes cooling of the gas, heat is removed from the magma, and a small amount of solidification takes place, with work done (98.5 J kg^{-1}) balanced by release of latent heat from the solidifying mass, 250 mg of solidified lava per kg of magma. Normally this would be totally negligible, but here it is distributed on the inside walls of bubbles. This increases the viscosity of the bubble walls and helps to retard further expansion. At the surface another effect helps to arrest the growth of bubbles. Immediately upon the exposure of hot magma to space, the upper surface is flash frozen due to the loss of heat by thermal emission. Thermal conduction rapidly propagates a chilling effect downward a few centimeters. Thus, in final assessment, the equations for bubble size cannot be extrapolated to the surface. Rather than having large size, the bubbles are of maximum diameter at a depth of about a centimeter. For the purpose of this study, we can take the bubbles at a depth of one centimeter to have radii of about 1 mm.

[41] The effect of bubbles rising in the magma is relatively small and can be ignored. The significance of this effect was assessed by applying Stoke's Law:

$$\mathrm{v} = \left(2\ \mathrm{g}\ \Delta\rho\ \mathrm{r}^2\right)/9\,\eta, \tag{6}$$

where v is the terminal, upward, velocity of a bubble, g is the acceleration due to gravity, $\Delta\rho$ is the density contrast between liquid and gas, r is the bubble radius, and η is the viscosity. At a depth of 10 cm a typical bubble radius is 0.5 mm. With a viscosity of 1500 Pa s for basalt, the ascent rate is 1.5 cm per day. At a depth of 1 m the ascent rate is about a factor of four less. However, there is an effect, which interferes with the free ascent of bubbles in magma. At temperatures near the solidus, magma tends to have a rather large weight percent of crystals. This causes the effective viscosity to be much higher than the value used in the above calculation, and the resulting velocities much slower. Perhaps it is not surprising that coalescence of bubbles rarely occurs. In 1974, Bennett pointed out "...that the high viscosities of magmas present a formidable barrier to bubble coalescence particularly when the flow fields of the liquid around neighboring bubbles interfere with one another. In order to expand, neighboring bubbles must force high-viscosity liquid along tortuous channels between expanding bubbles" (quoted from *Sparks* [1978]). This is further compounded when, as in our case, the melt has a rather large weight percent of crystals. Thus magma solidified at a given depth in the crust tends to have bubbles of a uniform size, a fact also borne out by terrestrial field observations.

[42] The texture of the sea crust has now been considered from a theoretical point of view and also by comparison with a terrestrial analogue. These suggest that a value of thermal conductivity, k, similar to that approximate for Hawaiian lava flows would be appropriate. The results of using these values of k are shown in temperature versus time plots in Figure 10. As shown in Table 2, we have adopted 0.9 W m^{-1} s^{-1} for the thermal conductivity. This value is consistent with the available Io data and compares well with the terrestrial analogue.

6. Temporal Evolution of Thermal Emission

[43] Using the resurfacing process we can calculate the thermal emission from all of Loki Patera over a resurfacing cycle. We integrate the thermal emission over the surface of the sea as the temperature distribution changes with time. The construction of this model is described in Appendix B. The evolution of the total thermal emission over a cycle is shown in Figure 11. The calculation was performed for an elliptical basalt lava lake with an area of 2.15×10^4 km^2, and a long axis of 196 km, which is resurfaced with a foundering wave that propagates across the lake with a velocity of 1 km per day. After 196 days the entire surface of the lake is replaced. The new crust then is allowed to cool for another 344 days. This time is set by the thermal conductivity of the crust. After 540 days the crust is thick enough and foundering begins again. Surface temperatures at the beginning of the cycle range from 250 K (crust thickness of 6.8 m) to 264 K (crust thickness of 5.4 m). Integrating thermal emission over the surface of the lake yields the total thermal emission as a function of time. The relationship between exposure time, surface temperature, and crust thickness, is described by *Davies* [1996] and in Appendix A.

[44] A similar modeling technique is used by *Rathbun and Spencer* [2005a] to show that the observed 3.5 or 3.8 μm flux from Loki Patera is quantitatively matched by the foundering model. *Rathbun and Spencer* [2005a] also considered the change in behavior of Loki Patera in 2001, and demonstrated that the new thermal flux could be explained by making small variations in the speed of the resurfacing front [*Rathbun and Spencer*, 2005b]. Foundering ultimately depends on the contrast between the bulk density of the crust and the liquid magma beneath. By making small variations in the porosity of the crust, the resurfacing model can match the observed thermal behavior at 3.5 μm. The resurfacing of Loki Patera is not a completely steady or smooth process, as evidenced by small variations in the age/distance profile shown by *Davies* [2003].

[45] It is illuminating to consider the total thermal emission from Loki Patera over, first, the course of one cycle (shown in Figure 11), and then over many cycles. The model's minimum thermal emission, 5.71 TW, is 6% of Io's total (10^{14} W). The maximum thermal emission is 15.6 TW, 16% of Io's total. The average thermal emission is 9.6 TW, or ~10% of Io's total. The range is wholly consistent with the observed range of thermal emission from Loki Patera as outputting 10–15% of Io's thermal emission [*Veeder et al.*, 1994]. The total thermal emission over 540 days is 4.5×10^{20} W.

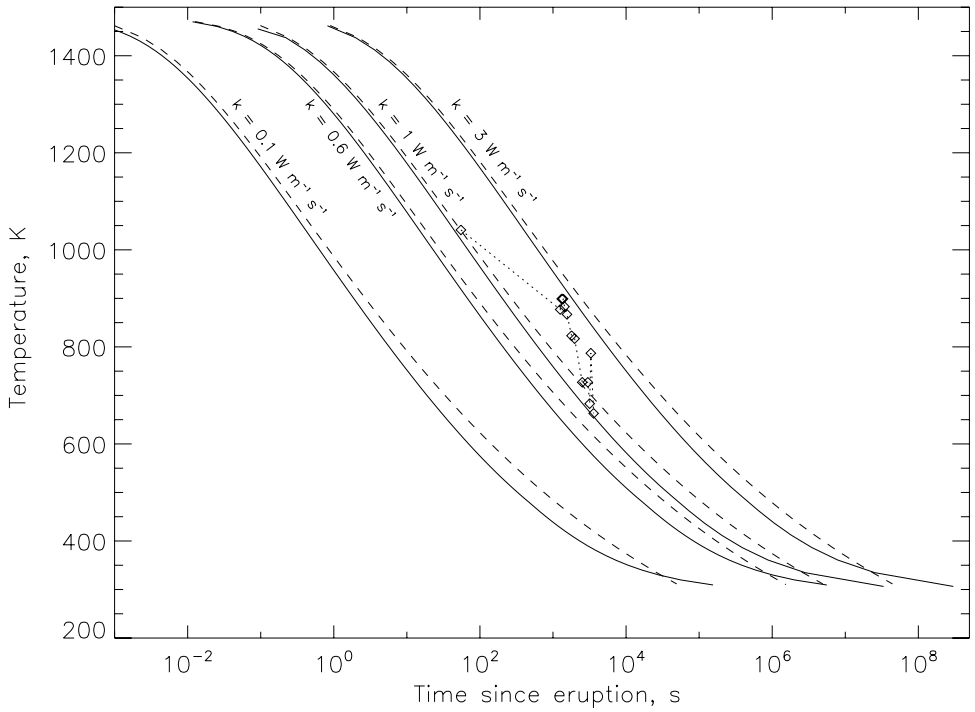

Figure 10. Effect of varying thermal conductivity on the cooling of lava on Io (dashed) and Earth (solid lines). The Earth model includes heat transport to and by a thick atmosphere [*Davies*, 1996]. The curve for thermal conductivity of 1 W m^{-1} s^{-1} compares well with cooling crust on a Hawaiian flow (dotted lines with diamonds) [*Flynn and Mouginis-Mark*, 1994]. For Io an allowance is made for higher porosity by using values for thermal conductivity similar to those for Hawaiian basalt, typically values from 0.6 to 0.9 W m^{-1} s^{-1}.

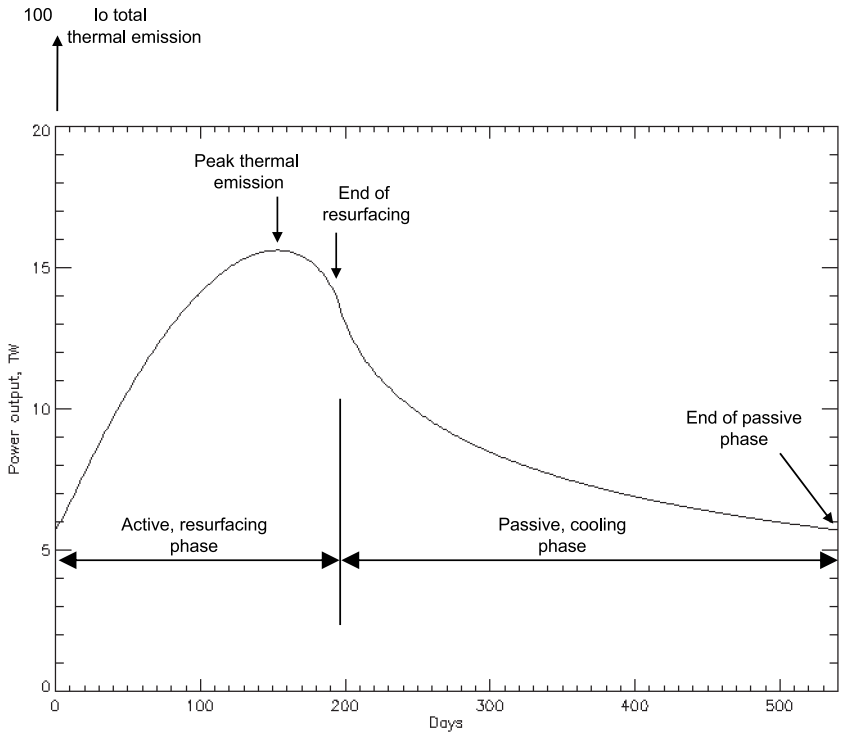

Figure 11. Variability of total thermal emission during the foundering and subsequent cooling of an elliptical lava lake (see Appendix B) with an area of 2.15 × 10^4 km^2, a long axis of 196 km, and a short axis of 140 km. The temperature of each 1-km wide surface area is calculated using the Io lava cooling curve for a semi-infinite body [*Davies*, 1996].

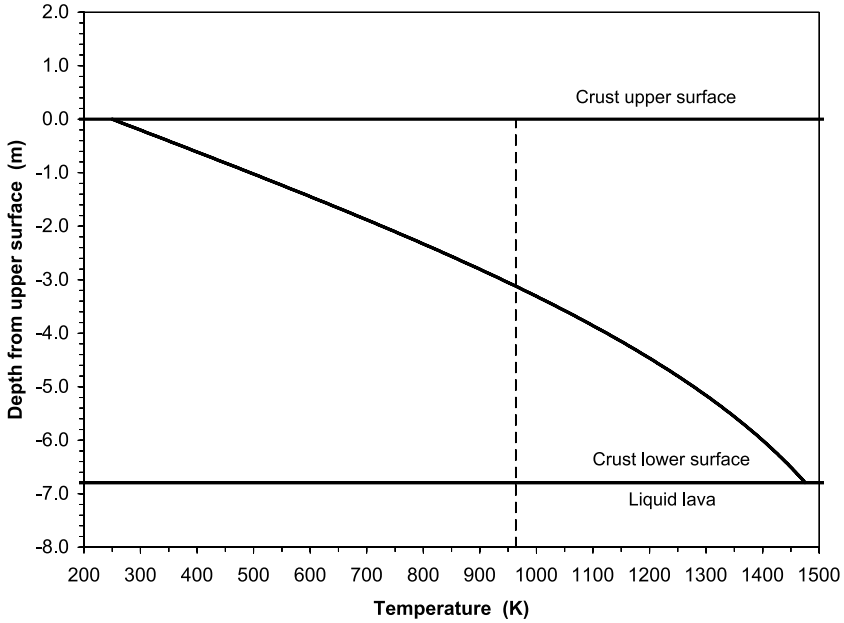

Figure 12. Temperature profile through the lava lake crust after 540 days, determined using *Head and Wilson* [1986] and *Davies* [1996]. At 540 days the bulk density of the crust exceeds that of the underlying liquid, and the crust founders [*Rathbun et al.*, 2002].

[46] The volume of the crust that forms and is subsequently destroyed during one 540 day cycle is given by

$$V = z\,A, \tag{7}$$

where A = area of the sea (2.15×10^{10} m^2) and z = thickness of crust after 540 days (= 6.8 m). V therefore is 146 km^3. If bulk density of the crust after 540 days ρ = 2600 kg m^3 and the mass m (kg) of the crust is

$$m = A\,z\,\rho, \tag{8}$$

then m = 3.80×10^{14} kg.

[47] The heat content of the crust, that is, the latent heat (Q_{latent}) liberated through solidification and the integrated sensible heat loss ($Q_{sensible}$) across the crust, from the final surface temperature of ~250 K to the liquidus temperature of 1475 K at the base of the crust, should be equivalent to the total observed heat loss (Q_{total}). For m = 3.80×10^{14} kg latent heat loss Q_{latent} (at 4×10^5 J kg^{-1}) is 1.52×10^{20} J.

[48] $Q_{sensible}$ is determined from the temperature profile through the crust at the moment of foundering, and is determined for the entire area of the lake (A) using

$$Q_{sensible} = A \sum_{x=0}^{x=z} \Delta T_x\, c\, V_{T,x}\, \rho, \tag{9}$$

where ΔT_x is the temperature difference between liquidus temperature and crust temperature at depth x; c is the specific heat capacity (1500 J kg^{-1} K^{-1}; $V_{T,x}$ is the volume of the crust at temperature T at depth x; and ρ is the crust bulk density. The temperature profile through crust 540 days old is shown in Figure 12. Integrating over the depth of the crust, the sensible heat loss is 1.37×10^{10} J m^{-2}, or 2.94×10^{20} J over the entire surface of the lake.

[49] Adding Q_{latent} to $Q_{sensible}$ from equation (9) yields Q_{total} = 4.46×10^{20} J. This value matches the modeled thermal output from Loki Patera over 540 days, described above, of 4.5×10^{20} J. The favorable comparison shows the internal consistency of the cooling model.

[50] This calculation shows that ~2000 km^3 of lava has solidified and foundered at Loki Patera in just the last 20 years (13.5 cycles), an average rate of 100 km^3 yr^{-1}. The total thermal emission over this interval is 6×10^{21} J, or 10% of Io's total thermal emission over this time.

[51] In summary, the foundering model matches observations of temperature distribution (and implied ages) and quantitative measurements of thermal emission over a wide wavelength range.

7. Foundering

7.1. Buoyancy

[52] "Freeboard" is the height at which a floating object protrudes above the surface of the liquid. In our model this is the distance between the top of the crust and the surface level of the molten part of the magma sea. When the buoyancy becomes zero, freeboard is also zero, and the surface of the crust is at sea level. The freeboard for the 5 and 10 m thick crusts is plotted in Figure 13.

[53] The crustal plates on the magma sea are relatively low-lying features, as Figure 13 shows. For the 5-m thick crust the maximum freeboard is only about 22 cm and for the 10-m thick crust it is about 44 cm. Negative freeboard in Figure 13 indicates negative buoyancy. How this can arise is discussed in the next section.

7.2. To Sink or Not to Sink?

[54] One might think that a crustal plate sinks when it achieves negative buoyancy. It is not that simple. For example, a plate simply might be held up by attachments to its neighbors. Not only might they be physical attachments, which must be broken, but the neighbors can impede the flow of liquid around the plate. How can a plate

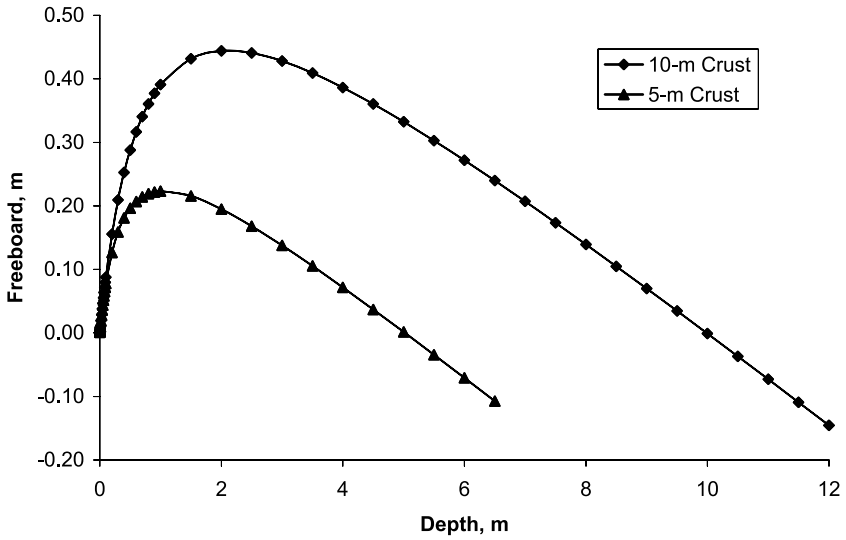

Figure 13. Freeboard as a function of crustal thickness for plates that become neutrally buoyant at thicknesses of 5 and 10 m. Properties are as per tabulation in Table 3.

submerge if liquid cannot cover it? When liquid lava does reach the top of a plate, it might freeze-upon contact, forming a small levee. Building levees along the whole perimeter would increase the buoyancy because, in effect, a boat has been created.

[55] The available thermal emission map for Loki Patera (Figure 5) has been interpreted to indicate that foundering of plates occurs as a chain reaction. A "wave" is inferred to propagate across the surface at a velocity of about 1 km day^{-1}. This suggests that the most likely mode of sinking is that of zero or negatively buoyant plates being pulled down by a neighbor [*Spencer et al.*, 2000; *Rathbun et al.*, 2002]. If foundering takes place exactly when zero buoyancy is reached, the only variable governing the time of foundering is then the age of the surface. From this point of view, if adjacent blocks are one day apart in age the latter will sink one day after the former.

[56] Just beneath the solid crust is a very viscous layer of magma. If the relative plate motion is not too fast, this layer can support some stress between the plates. Under these conditions, the plates behave somewhat like they would on a conveyor belt. Thus it may be that when a plate founders, the sinking plate can drag down the adjacent plate. The front thus propagates across the caldera at the same rate at which the original crust formed, some 1.5 years earlier. In another year and a half, this self-repeating process does the same thing again.

[57] The diurnal Jovian tide may assist in sinking crustal plates. We consider the tidal deformation and stresses developed at Loki Patera, and compare this with the tidal behavior of the adjacent crust. Thus we compute the differential tidal response of the magma sea and identify the potential effects on crustal plates. Io's tidal response as a whole is computed using numerical integration of the spheroidal oscillation equations as described by *Takeushi and Saito* [1972]. The eigenfunctions correspond to the tidal potential, the radial and tangential stresses and the radial and tangential deformation. The amplitude of the induced dynamic tide possible at Io's surface is presented in Figure 14 in terms of tidal potential percentage. With latitude 12.6°N and 309.9°W longitude, Loki Patera is located close to a maximum deformation area.

[58] A number of thermal evolution models have been proposed to account for Io's tidal dissipation (see *Zhang and Zhang* [2001] for a review of pre-Galileo models). A recent synthesis of the Galileo observations led *Keszthelyi et al.* [2004] to describe Io as having a molten core, a partially molten mantle, and a solid lithosphere on sufficient thickness to support Io's topography. Two thermal evolution models of Io are discussed by *Monnereau and Dubuffet* [2002, Figure 4]. The high-temperature model resembles that of *Keszthelyi et al.* [2004], while the cold model is globally solid and has high viscosity. The equivalent lithosphere is relatively thick. We used the model of *Keszthelyi et al.* [2004] for one extreme and the cold model of *Monnereau and Dubuffet* as the other. These are labeled "K2004" and "MD2002," respectively. For both models we computed the tidal response.

[59] Loki Patera itself is modeled as a two-layer body. The crust is elastic and 5 to 10 m thick (see Table 4). Below that is a liquid basaltic layer whose viscoelastic properties are presented in Table 2. We use Maxwell rheology [e.g., *Zschau*, 1978; *Segatz et al.*, 1988] to calculate tidal dissipation using the known orbital period and a basaltic material. We checked the results by computing tides for the whole body. The result agrees within less than a percent with *Segatz et al.* [1988] and *Bart et al.* [2004].

[60] Depending on the interior model, the differential tide between the magma sea and the adjacent lithosphere or country rock ranges from ±2 m (MD2002) to ±25 m (for K2004). The tides depend mainly on the lithospheric structure and the rheological properties of the first 300 kilometers beneath the surface (using properties in Table 2). Magma viscosity and surface crust thickness (within our model range) have little or no effect on the amplitude of the tide. Depth of sea from 10 to 30 km also has little effect.

[61] The amplitude of the magma sea tide is controlled by the tidal displacement of the rock at the seafloor. The presence of a deep, wide liquid body transmits the full

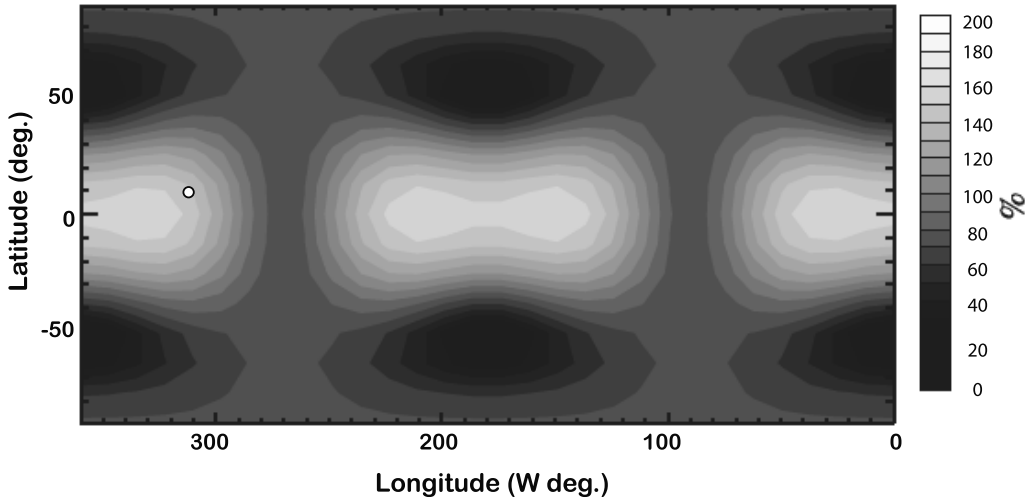

Figure 14. Relative tidal amplitude at the surface of Io with respect to the mean value over an orbit. Longitude is in degrees west. The relative deformation for Loki Patera is ~200%, independent of the interior model used. The amplitude (in meters) of the radial deformation ranges from ±2 m to ±2.5 m depending upon the model used for Io's interior. Loki Patera is indicated by the circle.

amplitude of the tide at the top of the asthenosphere to the surface [*Sohl et al.*, 1995].

[62] The tide produces a change in the surface area of Loki Patera as the figure of Io passes through various amounts of spherical oblateness. This amounts to about ±20 km^2 for each of the models, or a difference of 40 km^2 between high and low tide. This is about 0.2% of the floor area of Loki Patera.

[63] The vertical motion of the tide does not, by itself, offer many new ways to sink plates of sea crust. One

Table 4. Characteristics of the Loki Magma Sea Model

Property or Observation	Remarks	Value
Diameter	Observed	200 km
Depth	Bottom does not influence upper boundary of the sea.	unknown
Horizontal shape	Assumed to be the dark albedo surface of Loki Patera.	roughly circular, with high-albedo patch in center.
Magma kinematics	Initially static.	model evolves two phase convection
Magma temperature	Subsurface is isothermal.	1475 K, basalt liquidus[a]
Gas composition	Assumed.	SO_2
Gas content	Set by sea crust thicknesses of 5 and 10 m.	$n_{SO2} = 1.82 \times 10^{-5}$ and 3.62×10^{-5} mass fraction of SO_2
Surface temperature	Upper boundary.	varies, ~250 to 1475 K
Magma composition	Consistent with temperature observations	basalt
Thermal properties	Assumed on basis of composition. See *Davies et al.* [2001] for a tabulation.	appropriate for basalt
Vertical shape of surface	Hydrostatic surface.	1815 km radius of curvature
Surface smoothness	Specular reflection of sunlight observed. Surface may be flash-frozen, quenched glass.	smooth with respect to wavelength of visible light.
Heat flow	Matches observations	
Surface temperature distribution	Predicted by model.	as observed
Surface cooling rates	Predicted by model.	as observed
Temporal scale of activity	Predicted by model.	500–600 days
Rate of sea crust formation	For average T = 350 K (example).	emission = 1.79×10^{13} W crust forms at 2.6×10^4 m^3 s^{-1}, or 72,300 tonnes s^{-1}, or 100 km^3 yr^{-1}
Thickness of sea crust	At time of neutral buoyancy.	5–10 m
Mass of sinking plates	Total surface crust volume. After thermodynamic equilibrium.	146 km^3 per 540 day cycle 1.1×10^{15} kg, or 2.4×10^7 kg s^{-1}
Heat source	Unknown source.	steady supply
Foundering wave velocity	Variable from 2001.	1 km d^{-1} (1988–2000)

[a]Liquid to solid transition temperature used for thermodynamic calculations.

example might be if, at low tide, if a piece of crust becomes snagged on the edge of the caldera it will be pulled beneath the surface as the tide rises. When the change in area is combined with the vertical tide, irregularities in the edges of the crustal plates may snag other floaters and pull or push them downward during the compression cycle.

[64] At low tide all of the plates are jammed together. As the tide rises, additional area becomes available. This might involve the opening of cracks or other areas of weakness. One such region may be around the circumference of Loki Patera, as shown by the hotter surfaces in Figure 5. Molten magma will be exposed to space, albeit through a confined geometry. As heat is radiated to space, new, thin, crust forms. This continues until high-tide. Then the process reverses and area is lost. The crust is compressed. Where the crust is very thin, it can be crushed between the larger, thicker, crustal plates. The walls of the neighboring blocks are relatively porous at the level of the liquid surface. Thus the crushed material may be injected into the most porous part of the crust, collapsing pore space and in general reducing the porosity and adding mass to the plates. A net buoyancy decrease would result. On the next cycle, the crushed material remains in place and as cracks open, a new surface is solidified.

[65] As the freeboard of the plates becomes very low, inter-plate crust may be pushed up, on top of the thicker plates and contribute to initiating their foundering. When the buoyancy becomes zero or negative, there will be no restoring force that tends to return a plate to the surface. Thus it cannot recover from any downward push and will only continue to sink.

[66] The locations of recent founderings are particularly susceptible to changing area. Since the crusts are thin at these places, they are more vulnerable to being crushed at low tide. As the tide reverses, they would tend to be opened up again to fresh magma. Perhaps this effect may be responsible for some areas (e.g., the SW hot spot) tending to have high thermal emission more or less continuously.

7.3. "Bulking Up" of Sinking Sea Crust

[67] The sinking of sea crust plates initiates another process, which we can assess quantitatively. We call it "bulking up." Just before foundering the crust has a temperature of ~250 K on its top surface and ~1475 K on the bottom. The temperature profile in the crust is calculated using the method in Appendix A, and is shown in Figure 12. Immediately upon foundering a plate is surrounded by magma at 1475 K. Now the plate itself can be thought of as having a "heat deficit." All of the heat that it radiated to space while it was at the surface must now be replaced. Heat flows into the plate. Since the magma sea is isothermal, the inflowing heat is provided by latent heat of fusion. This comes from the solidification of additional magma onto the plate. For basalt, the plate agglomerates mass equal to ~190% of its mass at the time of foundering. This amount is calculated as follows. From the crust temperature profile (Figure 12), at the time of foundering, the average plate temperature is 963 K. The average temperature drop is therefore 512 K, which is a sensible heat loss of 7.7×10^5 J kg^{-1}. This heat loss in the sinking block is made up by latent heat released from the surrounding magma solidifying onto the block, at 4×10^5 J kg^{-1}. The accretion of 1.9 kg of basalt per kg of sinking crust is necessary to restore thermal equilibrium with the 1475 K magma. The total mass of the sinking material is now ~3 times the block mass at the time of foundering. This amounts to an average sinking rate of ~10^7 kg s^{-1} for Loki Patera as a whole. To this, add the mass of any liquid magma, which becomes entrained with the downward going plates. The process of agglomeration may take some time and may not have reached completion by the time the whole mass reaches the bottom of the sea. (At present the depth of the sea is unknown, but *Leone and Wilson* [2001] have suggested that magma chambers should be no deeper than about 30 km, and the average Io crustal thickness is assumed to be at least 30 km [e.g., *Jaeger et al.*, 2003]). Thus the foundering of crustal plates floating on the magma sea has led to the creation of a much larger, downward going mass, or plume (especially if some liquid magma becomes entrained with the sinking mass). Since these plumes are dominated by the higher density solid phase, they continue until they reach the bottom of the sea, or until they melt.

[68] To balance the downward flux, an equal amount of mass must move upward. We estimate that the whole (liquid) subsurface of Loki Patera is moving upward an average rate of 2–3 m yr^{-1}. Several caveats apply to this number. First it assumes that the bulking up process goes to completion. Thus this number is valid at a depth just below that at which bulking up has been completed. On the average, at shallower depths the velocity will be less because less mass is needed to counterbalance what was lost from that depth. The mass of the foundering plates sets the lower bound, which is at the surface.

[69] When the plates are floating they accrete mass on their bottom sides. In the region from the surface and extending to some unknown depth is another accretion zone. In this zone, surface plates grow by accretion, mostly upon what used to be their top.

8. Sinking Sea Crust Plates and the Source of Heat

[70] Whether or not the sinking slabs of sea crust actually reach the bottom of the magma sea is a profound question because it is linked to the source of heat for Loki Patera. While the answering of this question quantitatively is beyond the scope of this paper, we can, with the tools at hand, visualize some possible outcomes and identify the types of enhancements that would be needed for our model to attempt to address this question.

[71] Consider three cases: (1) no heat sources, (2) heat is supplied through the seafloor, and (3) heat is provided by uniform dissipation throughout the volume of the magma sea. The first case is adequately represented by the model defined in this paper. The descending slabs all reach the bottom where they find a huge jumble of plates that sank earlier. When the magma sea was created it started with an initial amount of heat. That amount is being diminished by thermal radiation to space. This will continue until the whole sea has solidified.

[72] In the second case, when heat is supplied from below the magma seafloor, a continuing steady state condition is possible. In this case the descending slabs reach the sea-

floor. There they absorb heat and melt. The resulting liquid is displaced upward as new slabs arrive on the seafloor.

[73] The third case envisions heat arising from uniform dissipation throughout the volume of the magma sea. The sinking slabs do not accrete as much mass as in the other cases because some of the heat needed comes directly from dissipation as well as from latent heat from accreting mass. After a slab has sunk deeply and no longer has a heat deficit, it will suffer erosion by melting as it encounters additional heat from dissipation at depth. Pieces of some of the slabs reach the bottom where eventually they melt.

[74] If less heat is supplied than is being radiated by Loki Patera then in both the second (seafloor source) and third (uniform dissipation) cases the descending slabs will reach the seafloor and form a debris layer. Over the long term, the sea may become shallower or reduce its areal extent. If heat is super-abundant and exceeds that being radiated, the volume of the sea may increase and ultimately the amount of power radiated from the surface will adjust to equal that supplied from depth.

9. Discussion

[75] The Magma Sea Model does well at matching all of the available observational data relevant to Loki Patera. It also provides a framework for the calculation of parameters for additional modeling of processes to better characterize the nature of Loki Patera and for predicting its future behavior. However, the accuracy of this idealized model hinges upon the accuracy of approximations and assumptions in the model. Assumptions meriting further discussion are the magmatic composition, concomitant viscoelastic properties, and the isothermal approximation.

[76] The possible presence on Io of sulfurous, basaltic, and ultramafic (mantle-like, high-Mg) lavas has been discussed in the literature and in section 2 of this paper. Observed temperatures of eruption are too high for sulfur and thus are sufficient to dismiss sulfur as a primary magma, though it probably plays a superficial, secondary role. Very high temperatures (e.g., above 1800 K) have not been observed at Loki Patera. Temperatures are instead consistent with basaltic lava. The wide availability of data for the properties of basalt is fortunate because many of the simulations that we have carried out would be impossible without the supporting base of laboratory and field data.

[77] The isothermal assumption was taken as a simplification to make the model tractable. On the one hand, if significant temperature differences arose, convection would set in and efficiently move heat to bring the bulk of the sea toward an isothermal state. On the other hand, in the absence of a temperature dependent rheological law any problems encountered must be handled on an ad hoc basis. Most serious of these is the amount of crystallization in the magma as the temperature approaches the solidus. A few degrees above the solidus the crystalline weight percent can approach fifty percent and the viscosity increases by an order of magnitude. Under these conditions, the model's use of ''instant kinematics'' does not properly characterize the behavior of the actual magma. To circumvent this problem, consider the following device. Arbitrarily reset the solidus temperature to a value 50 K higher to avoid the high-viscosity zone and set the isothermal temperature to this value. Compensate by decreasing the value of the latent heat by 50 times the specific heat capacity (c_p). This adjusts the latent heat, C_L, downward by 19% and energy is conserved. For lava starting near 1440 K and cooling to ~250 K this does not significantly change any of the results of the model.

[78] In addressing the rise of bubbles in the magma we used a simple Stokes Law calculation. For the origin of the bubbles we used empirical relationships in the literature [e.g., *Sparks*, 1978]. As the bubbles are brought up toward the surface, the ideal gas law was used to calculate their expansion. However, at porosities in excess of 50 percent or so (less than half a meter from the surface), this ad hoc treatment is no longer valid because it does not treat the relatively thin film, viscous flow of fluid between bubbles. To correct this problem we adopt the limit of 30 percent porosity suggested on the basis of field data and used by *Leone and Wilson* [2003].

[79] Another consequence of the absence of a rheological law is that we can only heuristically treat the descent of sinking crustal plates. Once some information is available as to the depth of the sea, the fate of sinking plates merits detailed treatment because, as we have concluded in this paper, it is a function of the nature of the heat source.

[80] A magma ocean is global in size. Its source of heat comes from planetary accretion and radioactive isotopes. The Magma Sea is much smaller and its heat comes from tidal dissipation. The magma oceans have been hypothesized to have existed early (e.g., ~4.3 By ago) in the history of the solar system whereas the Magma Sea is active today.

10. Summary

[81] While ultramafic magma cannot be conclusively ruled out in this location from existing data, Loki Patera exhibits many characteristics, in terms of observed temperatures and resurfacing mechanism, consistent with a basaltic magma sea.

[82] Once plates of sea crust have sunk below the surface we discover that they continue to accrete mass. Furthermore, their continued descent drives convection in the ''sea.'' At this stage, the Magma Sea model is well defined and we can use it in an analysis and in simulations of the resurfacing of Loki Patera. The results of these analyses allow us to conclude that foundering of crustal plates is the mechanism by which the surface of Loki Patera is renewed.

[83] In the course of our study of Loki Patera we have learned much from the Magma Sea model (section 4) and the simulations which it has facilitated. In section 2 the analysis of the currently available temperature data allowed us to conclude that the magma at Loki Patera is basaltic in character. It is about 200 km in diameter and has a smooth, hydrostatic surface. Freshly exposed magma radiates thermal emission intensely. Its surface is flash frozen to a thin glass layer. It quickly grows in thickness (section 5). For example, after about 30 hours its surface has cooled to 500 K, and its thickness is about 32 cm. By this time growth in thickness has slowed to about 1 μm s^{-1}. The cooling history of the sea crust surface was calculated (Appendix A, and Figure 6). After about three years the temperature is approaching 250 K, the crust is ~7 m thick and the growth rate is ~1.3 m yr^{-1} (growth rate is plotted in Figure 7).

[84] The magma is very undersaturated in SO_2 with a mass fraction of $\sim$1 to 4×10^{-5} (section 5.2). The dissolved gas content determines the porosity profile of the sea crust which in turn sets the thickness it can reach before foundering. Calculated porosities for depths greater than a meter are reasonable (Figure 8). At depths of less than a meter other effects become important and the porosity rarely exceeds 30 to 40 percent. When the SO_2 comes out of solution it forms bubbles with a radius of $\sim$10 μm. These grow slowly as the magma approaches the surface and reach radii of $\sim$1 mm (Figure 9). Most of the upward motion of bubbles is due to magma convection as the effect of the bubbles rising in the magma itself is small. The slow growth and rise of bubbles means that near a given depth the bubbles will tend to have a uniform size, as is also seen in field observations of terrestrial analogues.

[85] The plates of sea crust are relatively low-lying features on the sea (section 7.1; Figure 13). Their maximum freeboard varies from several tens of centimeters up to almost half a meter. The freeboard is reduced as the crust grows. However the exact time of sinking does not necessarily correspond to the moment when buoyancy becomes zero. Several effects can cause sinking to be earlier or later. There is some evidence (section 7.1; Figure 5) that plates tend to sink when their neighbors are foundering. We have found that there are at least two processes for transmitting forces between plates. The diurnal tide in the Loki magma sea leads to a peak-to-peak surface area change of about 40 km^2. At low tide plates can be pushed together and bonded somewhat by the debris between them (section 7.2). Also, the melt just below the bottom of the crust is very viscous. As plates separate this slow-yielding, viscous interface tends to transmit force from one plate to another (section 7.2). The loci of recent founderings are particularly sensitive to the tidally induced area change. Their crusts are thin and susceptible to crushing when the tide is low.

[86] We discovered that pieces of sinking sea crust have a thermal deficit. As they founder into a uniform 1475 K environment, heat flows into them. All of the heat that they radiated to space is now being replaced. The replacement heat comes from the latent heat that is liberated as magma solidifies on the exterior of the former piece of sea crust. When this ''bulking up'' process has been completed, the piece of crust will have $\sim$3 times the mass it had when it foundered (section 7.3). Thus the average amount of material sinking in the Loki magma sea at this depth is 1.3×10^7 kg s^{-1}. To counter this, magma must move upward at a rate of 3 m yr^{-1}.

[87] The ultimate fate of the sinking sea crust is found to depend upon the source of heat. If there is no heat source and Loki is operating on only its initial allocation of heat, then the pieces all pile up on the bottom of the sea. If the heat enters the sea via the seafloor, then the blocks will be melted and their material recycled. If the source is tidal dissipation in the sea, they will bulk up less and then start to dissolve. They may or may not reach the seafloor (section 8).

[88] Finally, we took up the resurfacing of Loki Patera. The Loki magma sea residing in the patera loses heat by radiation to space. That heat comes from the solidification of magma as the crust grows. On average the thermal emission is 9.6 TW or $\sim$10% of the total from Io. It can be as high as 15.6 TW and as low as 5.7 TW (section 6.2). The emission is modeled as a function of the crustal lifecycle, showing that variation is intrinsic to the model (Figure 11).

[89] Each possible resurfacing mechanism leaves a spatial distribution of temperature as its signature. Lava flows and versions of mobile crust were tested along with the Magma Sea model. The signatures for each process were simulated (Figure 3) and compared with data (Figures 4 and 5). Several of the mechanisms require additional, implausible, ad hoc assumptions. No assumptions are needed by the Magma Sea foundering mechanism. Thus, by elimination, we conclude that crustal foundering is the operative process for resurfacing Loki Patera. In the past twenty years (13.5 cycles) the volume of material cycled through Loki Patera's sea crust amounts to $\sim$2000 km^3!

Appendix A: Lava Surface Temperature, Thickness, and Age

[90] The following is adapted from *Davies et al.* [2005]. A treatment for determining the thickness of crust on a lava body as a function of both time and surface temperature was developed by *Head and Wilson* [1986], using a variation of the solution to the Stefan model of formation of ice on a freezing lake. From *Head and Wilson* [1986] the thickness C (m) of the crust at time t is given by

$$C = 2\lambda\sqrt{\kappa t}, \tag{A1}$$

where κ is thermal diffusivity of the lava (m^2 s^{-1}), and λ is a dimensionless quantity such that

$$\frac{L\sqrt{\pi}}{c(T_S - T_0(t))} = \frac{\exp(-\lambda^2)}{\lambda erf(\lambda)}, \tag{A2}$$

where T_s is the magma liquidus temperature (K), $T_0(t)$ is the surface temperature (K) of the flow at time t, c is specific heat capacity (J kg^{-1} K^{-1}), L is latent heat capacity (J kg^{-1}) and *erf* is the error function. The heat flow through the surface of the lava flow is equal to the temperature gradient at the surface multiplied by the thermal conductivity of the lava, and must be equal to the total heat loss F (W m^{-2}) by radiation from the upper surface such that

$$F = \frac{k(T_S - T_0(t))}{\sqrt{\pi\kappa t}\, erf(\lambda)}, \tag{A3}$$

where k is thermal conductivity (W m^{-1} K^{-1}).

[91] The method of solution is as follows. A surface temperature $T_0(t)$ is selected and the left-hand side of equation (A2) solved, using thermophysical values for basalt, given in Table 2. The right-hand side of equation (A2) is solved iteratively to find λ, which is used with the value of $T_0(t)$ in equation (A3) to find time t, the time from commencement of cooling. The derived values of t and λ are then used in equation (A1) to find the crustal thickness at time t for surface temperature $T_0(t)$. The temperature profile within the crust at time t is determined as follows. Crustal thickness and cooling time are used in equation (A1)

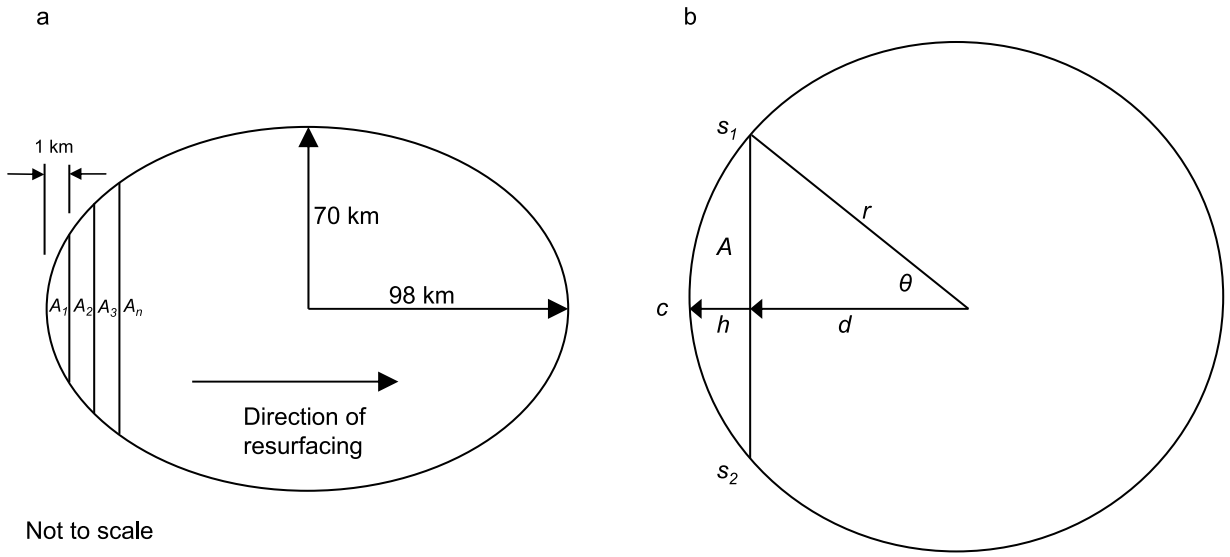

Figure B1. Calculation of model areas that are renewed as resurfacing sweeps across the floor of Loki Patera. The total emitting area used in the model is 2.15×10^4 km. The length of the lava sea is fixed at 196 km, and the surface wave propagates at 1 km per day, as shown in Figure B1a. The area of a circle with a diameter of 196 km is 3×10^4 km, 1.4 times the required area. The width of each area bin is divided by 1.4 to produce an ellipse with an area of 2.15×10^4 km^2. Figure B1b shows how the area of each segment is calculated. Radius $r = 98$ km. h is the distance from midpoint of chord to midpoint of arc; in this example, $h = 1$ km. S is length of arc ($s_1 - c - s_2$); θ is angle in radians of central angle subtending arc; c is length of chord ($s_1 - s_2$); and A is area of the chord. $d = r - h$, and $\theta = 2\ \mathrm{acos}(d/r)$, so $c = 2\ r\ \sin(\theta/2)$. $S = r\ \theta$, and $A = r^2(\theta - \sin(\theta))/2$. At the end of day 1 of resurfacing, the area renewed A_1 is calculated as shown. At the end of day 2 the area renewed A_2 is calculated by setting $h = 2$ km and subtracting A_1. Areas are then divided by 1.4 to correct total area. This process is repeated until the center of the ellipse is reached. Of course, $A_{196} = A_1$, $A_{195} = A_2$, $A_{194} = A_3$, etc., or, for $n = 1$ to 98, $A_{196\text{-}n} = A_n$. If the lake is rectangular, the area of each element is 1 km × width of the lake in km. *Rathbun and Spencer* [2005a, 2005b] model Loki Patera as rectangular, with a length of ~200 km.

to determine λ. Temperature T_x in the crust as a function of depth x is given by

$$T_x = \left[\left(\frac{T_S - T_0(t)}{erf(\lambda)}\right) erf\left(\frac{x}{2\sqrt{\kappa t}}\right)\right] + T_0(t). \qquad \text{(A4)}$$

[92] The derived relationship between surface age and surface temperature, shown in Figure 6, can now be used to model how thermal emission by radiation changes with time.

Appendix B: Lava Lake Thermal Emission and Evolution

[93] The lava lake thermal emission model used here is a variation of the *Davies* [1996] model for determining volcanic thermal emission for lava lakes and flows on Io. The *Davies* [1996] model incorporated a moving crust (the "mobile crust" model described in this paper), and was modified to replace areas of crust in situ without lateral crustal movement, to simulate foundering. A similar model has been developed by *Rathbun and Spencer* [2005a, 2005b].

[94] The evolution of the thermal emission from the Loki Patera magma sea is determined as follows. The resurfacing model assumes that the foundering wave progresses across the patera at a rate of 1 km per day [*Rathbun et al.*, 2002; *Davies*, 2003]. The area of the low-albedo floor of Loki Patera is modeled as an ellipse with a long axis of 196 km and a short axis of 140 km, a total area of 2.15×10^4 km^2. A resurfacing wave sweeps across this area, approximating a resurfacing wave sweeping diagonally across the patera, which is 198 km across, replacing the total area in 196 days. On each new day, a new surface area is produced. The area of each segment is defined by a strip across the ellipse that is 1 km wide. The construction used to determine the area of each segment is shown in Figure B1. The area of each segment is shown in Figure B2. At the end of active resurfacing the surface at the SW end of the patera is 196 days old and 1 day old at the opposite end of the magma sea. Cooling of the crust continues for another 344 days before crust renewal begins again. The duration of an entire resurfacing and cooling cycle is 540 days, to match observations [*Rathbun et al.*, 2002].

[95] Using the age-temperature relationship described in the manuscript and shown in Figure 6, the temperature of each area bin T_i (K) is determined for each day. The total thermal emission $F_{(\lambda,T),i}$ as a function of wavelength λ (microns) is determined by the Planck function, so that

$$F_{(\lambda,T),i} = \sum_{i=1}^{i=n} \frac{c_1 A_i \varepsilon}{\lambda^5}\left(\frac{(1-f)}{\left(e^{c_2/\lambda T_i} - 1\right)} + \frac{f}{\left(e^{c_2/\lambda T_{liquidus}} - 1\right)}\right), \qquad \text{(B1)}$$

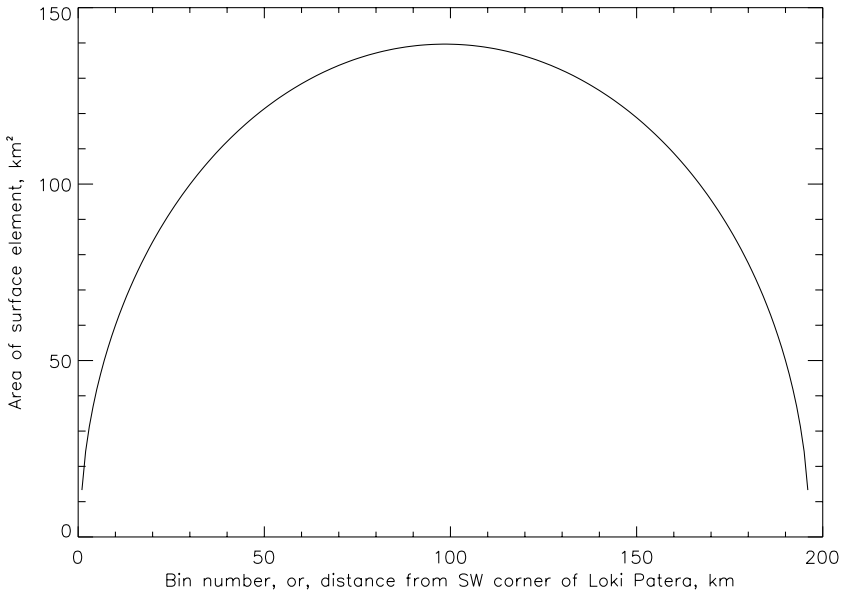

Figure B2. The area of each surface element for an ellipse of long axis 196 km and short axis 140 km, with a total area of 2.15×10^4 km^2 equivalent to the low-albedo area of Loki Patera, determined using the construction in Figure B1. As the resurfacing wave moves across the magma sea, each area is replaced.

where n is the number of bins (= 196), the area of each bin is A_i (km^2), and the age increment is one day. $c_1 = 3.7413 \times 10^8$ W μm^4 m^{-2}, and $c_2 = 1.4388 \times 10^4$ μm K. f is a lava crust crack fraction at lava eruption temperature $T_{liquidus}$ (K), set here to zero as Loki Patera is relatively quiescent and does not emit energy at short wavelengths consistent with exposure of significant incandescent lava.

[96] The model is first run for a cycle of 540 days to initialize the temperature distribution, and then run again. Each surface element is replaced and ages after the resurfacing wave moves on, and other elements allowed to age until replaced. Integrating over the entire magma sea surface yields the total thermal emission spectrum, and the area under the spectrum is the total thermal emission at that time. The evolution of total thermal emission is shown in Figure 11.

[97] **Acknowledgments.** The inspiration for the model developed in this paper came from a presentation by Gerry Schubert at the Fall Meeting of the American Geophysical Union in San Francisco [*Schubert et al.*, 2003]. They concluded that the available data for Io's shape was consistent with a hydrostatic figure. This, in turn, inspired our concept of a "magma sea" whose surface follows the global, hydrostatic figure of Io. "Back of the envelope" calculations suggested that such a model could explain the available thermal emission observations of Loki Patera and other data. The results of those calculations were presented at the 2004 Lunar and Planetary Science Conference [*Matson et al.*, 2004] and elaborated upon the following year [*Veeder et al.*, 2005]. The present paper provides a more detailed development of that model. The magma sea model has the advantages of being relatively simple and amenable to quantitative evaluation. We are indebted to Jani Radebaugh and Giovanni Leone for their detailed reviews. This work was carried out at the Jet Propulsion Laboratory, California Institute of Technology, under a contract from NASA. D.L.M., G.J.V., and A.G.D. are supported by grants from the NASA Planetary Geology and Geophysics Program. J.A.R. is supported by a grant from the NASA Outer Planets Research Program. J.C.C. is a Caltech Postdoctoral Scholar at JPL.

References

Bart, G. D., E. P. Turtle, W. L. Jaeger, L. Keszthelyi, and R. Greenberg (2004), Ridges and tidal stresses on Io, *Icarus*, *169*, 111–126, doi:10.1016/j.icarus.2004.01.003.

Carr, M. H. (1986), Silicate volcanism on Io, *J. Geophys. Res.*, *91*, 3521–3532.

Davies, A. G. (1996), Io's volcanism: Thermophysical models of silicate lava compared with observations of thermal emission, *Icarus*, *124*, 45–61, doi:10.1006/icar.1996.0189.

Davies, A. G. (2001), Volcanism on Io: The view from Galileo, *Astron. Geophys.*, *42*, 10–15, doi:10.1046/j.1468-4004.2001.42210.x.

Davies, A. G. (2003), Temperature, age and crust thickness distributions of Loki Patera on Io from *Galileo* NIMS data: Implications for resurfacing mechanism, *Geophys. Res. Lett.*, *30*(21), 2133, doi:10.1029/2003GL018371.

Davies, A. G., J. Radebaugh, L. P. Keszthelyi, A. S. McEwen, and the Galileo NIMS and Cassini ISS Teams (2001), Temperature-area determination from observations of Loki by *Galileo* and *Cassini*, *Bull. Am. Astron. Soc.*, *33*, 5.07.

Davies, A. G., D. L. Matson, G. J. Veeder, T. V. Johnson, and D. L. Blaney (2005), Post-solidification cooling and the age of Io's lava flows, *Icarus*, *176*, 123–137, doi:10.1016/j.icarus.2005.01.015.

Flynn, L. P., and P. J. Mouginis-Mark (1994), Temperatures of an active lava channel from spectral measurements, Kilauea Volcano, Hawaii, *Bull. Volcanol.*, *56*, 297–301.

Flynn, L. P., P. J. Mouginis-Mark, J. C. Gradie, and P. G. Lucey (1993), Radiative temperature measurements at Kupaianaha lava lake, Kilauea Volcano, Hawaii, *J. Geophys. Res.*, *98*, 6461–6476.

Geissler, P. E., A. S. McEwen, L. P. Keszthelyi, R. Lopes-Gautier, J. Granahan, and D. P. Simonelli (1999), Global color variations on Io, *Icarus*, *140*, 265–282, doi:10.1006/icar.1999.6128.

Geissler, P., A. S. McEwen, C. Phillips, L. Keszthelyi, and J. Spencer (2004), Surface changes on Io during the Galileo mission, *Icarus*, *169*, 29–64, doi:10.1016/j.icarus.2003.09.024.

Greeley, R., E. Theilig, and P. Christensen (1984), The Mauna Loa sulfur flows as an analog to secondary sulfur flows (?), *Icarus*, *60*, 189–199.

Gregg, T., and R. Lopes (2004), Lava lakes on Io: New perspectives from modeling, *Lunar Planet. Sci.*, *XXXV*, 1558.

Head, J. W., and L. Wilson (1986), Volcanic processes and landforms on Venus: Theory, predictions, and observations, *J. Geophys. Res.*, *91*, 9407–9446.

Howell, R. R. (1997), Thermal emission from lava flows on Io, *Icarus*, *127*, 394–407, doi:10.1006/icar.1997.5686.

Jaeger, W. L., E. P. Turtle, L. P. Keszthelyi, J. Radebaugh, A. S. McEwen, and R. T. Pappalardo (2003), Orogenic tectonism on Io, *J. Geophys. Res.*, *108*(E8), 5093, doi:10.1029/2002JE001946.

Johnson, T. V., G. J. Veeder, D. L. Matson, R. H. Brown, and R. M. Nelson (1988), Io—Evidence for silicate volcanism in 1986, *Science*, *242*, 1280–1283.

Keszthelyi, L., and A. McEwen (1997), Magmatic differentiation of Io, *Icarus*, *130*, 437–448, doi:10.1006/icar.1997.5837.

Keszthelyi, L. P., W. L. Jaeger, E. P. Turtle, M. Milazzo, and J. Radebaugh (2004), A post-Galileo view of Io's interior, *Icarus*, *169*, 271–286, doi:10.1016/j.icarus.2004.01.005.

Leone, G., and L. Wilson (2001), Density structure of Io and the migration of magma through its lithosphere, *J. Geophys. Res.*, *106*(E12), 32,983–32,996.

Leone, G. L., and L. Wilson (2003), Links between depths of magma reservoirs and volcanic eruption rates on Io, *Lunar Planet. Sci.*, *XXXIV*, 1685.

Lopes, R. M. C., et al. (2004), Lava lakes on Io: Observations of Io's volcanic activity from Galileo NIMS during the 2001 fly-bys, *Icarus*, *169*, 140–174, doi:10.1016/j.icarus.2003.11.013.

Lopes-Gautier, R., et al. (1999), Active volcanism on Io: Global distribution and variations in activity, *Icarus*, *140*, 243–264, doi:10.1006/icar.1999.6129.

Lopes-Gautier, R., et al. (2000), A close-up look at Io from Galileo's Near-Infrared Mapping Spectrometer, *Science*, *288*, 1201–1204.

Lunine, J. I., and D. J. Stevenson (1985), Physics and chemistry of sulfur lakes on Io, *Icarus*, *64*, 345–367.

Matson, D. L., A. G. Davies, G. J. Veeder, J. A. Rathbun, and T. V. Johnson (2004), Loki patera as the surface of a magma sea, *Lunar Planet. Sci.*, *XXXV*, 1882.

McEwen, A. S., D. L. Matson, T. V. Johnson, and L. A. Soderblom (1985), Volcanic hot spots on Io: Correlation with low-albedo calderas, *J. Geophys. Res.*, *90*, 12,345–12,379.

McEwen, A. S., D. P. Simonelli, D. R. Senske, K. P. Klaasen, L. Keszthelyi, T. V. Johnson, P. E. Geissler, M. H. Carr, and M. J. S. Belton (1997), High-temperature hot spots on Io as seen by the Galileo solid state imaging (SSI) experiment, *Geophys. Res. Lett.*, *24*(20), 2443–2446.

McEwen, A. S., et al. (1998), Active volcanism on Io as seen by Galileo SSI, *Icarus*, *135*, 181–219, doi:10.1006/icar.1998.5972.

Monnereau, M., and F. Dubuffet (2002), Is Io's mantle really molten?, *Icarus*, *158*, 450–459, doi:10.1006/icar.2002.6868.

Mysen, B. O. (1977), Solubility of volatiles in silicate melts under the pressure and temperature conditions of partial melting in the upper mantle, in *Magma Genesis: Proceedings of the American Geophysical Union Chapman Conference on Partial Melting in the Upper Mantle*, *Bull. 96*, edited by H. J. B. Dick, pp. 1–15, State of Oreg. Dept. of Geol. and Miner. Ind., Portland.

Rathbun, J. A., and J. R. Spencer (2005a), Loki, Io: Groundbased observations and a model for periodic overturn, *Lunar Planet. Sci.*, *XXXVI*, 1981.

Rathbun, J. A., and J. R. Spencer (2005b), Loki, Io: A model for the change from periodic behavior, *Bull. Am. Astron. Soc.*, *37*, 58.15.

Rathbun, J. A., J. R. Spencer, A. G. Davies, R. R. Howell, and L. Wilson (2002), Loki, Io: A periodic volcano, *Geophys. Res. Lett.*, *29*(10), 1443, doi:10.1029/2002GL014747.

Sagan, C. (1979), Sulphur flows on Io, *Nature*, *280*, 750–753.

Schubert, G., J. D. Anderson, R. A. Jacobson, E. L. Lau, W. B. Moore, and J. Pagulta (2003), Geodesy of Amalthea and the Galilean satellites of Jupiter, *Eos Trans. AGU*, *84*(46), Fall Meet. Suppl., Abstract G42C-01.

Segatz, M., T. Spohn, M. N. Ross, and G. Schubert (1988), Tidal dissipation, surface heat flow, and figure of viscoelastic models of Io, *Icarus*, *75*, 187–206, doi:10.1016/0019-1035(88)90001-2.

Smith, B. A., et al. (1979a), The Jupiter system through the eyes of Voyager 1, *Science*, *204*, 951–971.

Smith, B. A., et al. (1979b), The Galilean satellites and Jupiter: Voyager 2 imaging science results, *Science*, *206*, 927–950.

Sohl, F., W. D. Sears, and R. D. Lorenz (1995), Tidal dissipation on Titan, *Icarus*, *115*, 278–294.

Sparks, R. S. J. (1978), The dynamics of bubble formation and growth in magmas: A review and analysis, *J. Volcanol. Geotherm. Res.*, *3*, 1–37.

Spencer, J. R., J. A. Rathbun, L. D. Travis, L. K. Tamppari, L. Barnard, T. Z. Martin, and A. S. McEwen (2000), Io's thermal emission from the Galileo Photopolarimeter-Radiometer, *Science*, *288*, 1198–1201.

Takeushi, H., and M. Saito (1972), Seismic surfaces waves, in *Methods in Computational Physics*, vol. 11, edited by B. Alder et al., pp. 217–295, Elsevier, New York.

Turtle, E. P., et al. (2004), The final Galileo SSI observations of Io: Orbits G28–I33, *Icarus*, *169*, 3–28.

Veeder, G. J., D. L. Matson, T. V. Johnson, D. L. Blaney, and J. D. Goguen (1994), Io's heat flow from infrared radiometry: 1983–1993, *J. Geophys. Res.*, *99*, 17,095–17,162.

Veeder, G. J., D. L. Matson, J. A. Rathbun, A. G. Davies, and T. V. Johnson (2005), Loki Patera: An Io sea story, *Lunar Planet. Sci.*, *XXXVI*, 1587.

Williams, D. A., R. Greeley, R. Lopes, and A. G. Davies (2001), Evaluation of sulfur flow emplacement on Io from Galileo data and numerical modeling, *J. Geophys. Res.*, *106*(E12), 33,161–33,174.

Wright, T. L., and R. T. Okamura (1977), Cooling and crystallization of tholeiitic basalt, 1965 Makaopuhi lava lake, Hawaii, *U.S. Geol. Surv. Prof. Pap.*, *1004*, 78 pp.

Wright, T. L., W. T. Kinoshita, and D. L. Peck (1968), March 1965 eruption of Kilauea volcano and the formation of Makaopuhi lava lake, *J. Geophys. Res.*, *73*, 3181–3205.

Zhang, H., and C.-Z. Zhang (2001), The figure dynamical parameters of Io inferred from internal structure models, *Chin. J. Astron. Astrophys.*, *1*, 275–280.

Zschau, J. (1978), Tidal friction in the solid earth: Loading tides versus body tides, in *Tidal Friction and the Earth's Rotation*, edited by P. Brosche and J. Sundermann, pp. 62–94, Springer, New-York.

J. C. Castillo, A. G. Davies, T. V. Johnson, D. L. Matson, and G. J. Veeder, Jet Propulsion Laboratory, MS 183-501, 4800 Oak Grove Drive, Pasadena, CA 91109-8099, USA. (ashley.g.davies@jpl.nasa.gov)

J. A. Rathbun, Department of Physics, University of Redlands, 1200 East Colton Avenue, Redlands, CA 92373, USA.